DISCLAIMER:

This document does not meet the current format guidelines of the Graduate School at The University of Texas at Austin.

It has been published for informational use only.

The Report Committee for Marcellinus Azuka Ojinnaka

Certifies that this is the approved version of the following report:

Development of Real-Time Early Gas Kick Detection Model

APPROVED BY

SUPERVISING COMMITTEE

Supervisor: _____

Joseph J. Beaman Jr.

_____

Scott Fish

Development of Real-Time Early Gas Kick Detection Model

by

Marcellinus Azuka Ojinnaka, B.E.

Report

Presented to the Faculty of the Graduate School of

The University of Texas at Austin

in Partial Fulfillment

of the Requirements

for the Degree of

Master of Science in Engineering

The University of Texas at Austin

August 2013

To

my mom, **Felicia**, and my brother, **Steven**

Acknowledgements

I am very grateful to my supervisor, Dr Joseph Beaman, for his support, guidance and tutelage. I would also like to thank Dr Scott Fish for the review of the text and his many insights and suggestions. This work was financially supported by British Petroleum.

August 2013

Abstract

Development of Real-Time Early Gas Kick Detection Model

Marcellinus Azuka Ojinnaka, M.S.E.

The University of Texas at Austin, 2013

Supervisor: Joseph Beaman

Gas kicks occur during oil and gas drilling operations due to pressure imbalances between reservoir pressure and bottomhole pressure. Uncontrolled gas kick results in blowouts which has severe consequences including death of rig personnel. For deepwater, High Temperature High Pressure, and depleted wells, early gas kick detection may mean the difference between a successful drilling operation and a catastrophic drilling operation. Modeling the physics of gas kicks is therefore an important aspect of well control in order to detect kicks and raise appropriate alarms that demand remedial action from the rig team. Also important is the quantification of the amount of kick already in the annulus and an estimation of the kick front, all in real time.

Various kick models have been developed over the years to model wellbore-reservoir interactions and aid early detection of gas kicks. Some of these models and simulators are numerical and analytical; others are based on extensive collection of well data of kick events to model drilling events signatures including kicks of various sizes. In general, for non-data driven models, the accuracy of models depends on the amount of simplification done and the validity of the assumptions made. Steady state, semi-steady state and transient models exist, but if accurate detection is to occur in real-time, it is crucial that transient models are used, that the assumptions are valid, and that over-simplification is avoided in order to reflect as closely as possible, the complex physics of wellbore-reservoir interactions. The important issues to consider include the type of fluid property model used, such as compositional or black oil models; the type of frictional model used, such as Power law or Bingham plastic model; the flow regime considered; slip velocity between the phases, and the extent to which first principles are applied to problem solving, as opposed to using correlations.

Our study is on real-time estimation of gas kicks during drilling using a two-phase, fully implicit, transient flow model in a vertical wellbore. The wellbore and reservoir are coupled, and a pressure gradient is introduced at the bottomhole causing gas influx into the wellbore. The gas front is then monitored in real-time as it is transported in the circulating mud to the surface pits. The model equations are the mud and gas continuity equations, the momentum conservation equation as well as sub-models, consisting of state equations and two-phase flow correlations, where needed.

Much of the complex physics of gas kick is modeled, and the outcome of this research provides a tool for gas kick prediction, detection and control, and also for the estimation of the volume of kick occurring at the bottomhole in real-time.

Table of Contents

List of Figures

Chapter 1: Introduction

Gas kicks are unwanted influxes from the reservoir into the wellbore during oil and gas drilling, tripping, and well completion operations. Drilling mud and drilling cement provide a barrier against pressurized hydrocarbons in the reservoir to contain fluids and keep them sealed in the reservoir until production commences. Drilling operations and unanticipated high pressure gas pockets however, can lead to pressure imbalances between wellbore fluids and reservoir fluids, causing gas influx into the wellbore or loss of drilling mud into the reservoir. The latter scenario is called lost circulation. If uncontrolled, both of these cases can lead to blowouts, which are usually catastrophic in nature, result in huge financial losses and even human casualty, and are extremely difficult and expensive to control.

Early gas kick detection is therefore critical to the prevention of blowouts. Most companies have standard well control procedures in place that are activated when the drilling crew observe and reach a conclusion that a kick event is ongoing. This is often after installed well monitoring systems raise alarms to signal the detection of a kick event. Hence without kick detection there can be no well control and blowouts would result. Therefore kick detection is the starting point of well control. Well monitoring applications use kick models developed analytically, numerically or through data collection and model-matching of signature trends of drilling events and anomalies. The accuracy and reliability of these applications in detecting gas kicks are only as good as the soundness of the models used.

Even though blowouts have been around since the advent of oil and gas drilling and production, and a lot of effort has been directed at gas kick studies, modeling and simulation, challenges still remain in modeling, simulating and detecting gas kicks. There are complex interactions between the liquid and gas phases during flow, some of which are either not fully understood, or are difficult to simulate. The flow and volume

measurement devices themselves come with uncertainties in their measurements and sometimes suffer accuracy problems. An example is the paddle wheel used to measure outflow rate at the return line near the mud pit. Fluid composition is different for every field and fluid models are varied and complex. It would be difficult to develop a well monitoring application tailor-made to accounts for the differences, both subtle and stark, of each individual field. Hence the use of calibration factors in some applications. This is necessarily error-prone, and could be time consuming. In addition, it could have been built on correlations which obscure the physics of flow interactions and wellbore-reservoir coupling.

These complexities have led to an over-simplification, as used in some gas models. For example, some models do not acknowledge slip velocity between the gas and liquid phases, while also assuming a homogenous mixture for friction pressure loss calculations. Other more detailed models have incorporated much of the complex physics in the flow and coupling interactions, making fewer and more valid assumptions, but still require measuring devices for flow and pressure measurements. These, naturally, have uncertainty and accuracy and reliability issues.

Our objective is to develop a comprehensive two-phase gas kick detection model for Water Based Muds (WBM) from a physics-based perspective, which has the salient physics of the process, and which can be applied to the prediction of gas influx volume at the point of entry of gas in real time.

The gas kick simulator developed is a unidirectional, fully implicit, staggered grid, black-oil, transient model. A finite volume approach is used to compute mud and gas pressures, mud and gas velocities, and gas volume fraction within the annulus of the wellbore, from the bottomhole to the surface and from the time of gas influx into the wellbore to its discharge at the surface, all in real-time. The Newton iteration technique is applied in the solution of the discretized equations since the equations present a

large, sparse, non-linear system of equations. The simulator can thus be used as a kick detection tool, a basis for estimating the volume of gas influx at the bottomhole, and provide a basis for the simulation of other mud types such as Oil Based Muds (OBM), and fluid flows with additional complexities such as compositional models, inclined wells and the different pressure loss calculation models.

The following paragraphs provide an overview of the remaining chapters and materials covered therein.

Chapter 2 provides a literature review on the state of the art of kick detection as obtains in the industry today. It is accompanied with a discussion of the strengths and limitations of each method, the kind of model and some of the general assumptions used, as well as a general discussion of the principles of gas kick detection.

Chapter 3 focusses on the mathematical relationships linking the variables and parameters as developed from first principle conservation laws. Sub-model equations used for flow parameters are highlighted. An attempt is made to list the flow interactions captured in the model as well as assumptions made. The transient model is discretized and a solution method is proposed.

Chapter 4 explores other means of solving the partial differential equations directly through Matlab toolboxes and industry-wide simulation suites. The advantages and limitations of these methods are discussed.

Chapter 5 provides a summary of the work, the conclusions reached, and recommendations for future work.

Chapter 2: Background and Literature Review

The subject of gas kicks dates as far back as the genesis of oil drilling itself. In those early days of drilling oil onshore, blowouts, called gushers, were a common sight in oil fields. They were often left to peter out uncontrolled. As technology improved, massive reservoirs have been discovered offshore in both shallow water (less than 500ft) and deep water and oil drilling has followed the same pattern. The consequences of blowouts have therefore increased. The huge economic losses and environmental damages incurred if a gas kick event is left uncontrolled and results in a blowout have provided the impetus for researchers to seek means for both early gas kick detection and well control.

2.1 WHY GAS KICKS OCCUR

Gas kicks are unwanted influx from the reservoir as a result of pressure imbalance between wellbore pressure and formation pressure. When reservoir gas enters the wellbore, it rises up the annulus either as free gas or dissolved gas in drilling mud. As it encounters lower pressure regions at the top of the annulus, it expands. Simultaneously, dissolved gas comes out of solution. The result is an increase in both gas and mixture velocity when leaving the annulus. If left uncontrolled, blowouts may result. Reservoir pressure is balanced by the hydrostatic head of the drilling fluid at the bottomhole while drilling and tripping, and drilling cement provides a barrier holding back reservoir fluid during well completions. Figure 2.1 shows the basic arrangement of wellbore, reservoir, and drilling equipment in a rig.

A corollary of gas kick is lost circulation. In this case drilling mud is lost to the formation as a result of the bottomhole pressure of the wellbore being greater than the reservoir pressure. This situation is called overbalance. If not remedied in time, it could lower pressure in the well bore annulus as a result of low fluid level. This could result in

an underbalance, a condition favorable to kick gas subsequently entering the wellbore from gas pockets somewhere further up the annulus [2].

Continuous drilling for over two centuries and a half has depleted reservoirs in easier to reach areas. The increasing demand for energy has led to oil exploration in virgin territories resulting in Deep Water wells, High Pressure High Temperature wells (HPHT) and Depleted wells. These come with new challenges because of water depth, narrow geo-pressure margins, and slimmer/ lower volume wells. Hence the need for greater accuracy, sensitivity and reliability in early kick detection and well control equipment [3, 4].

Gas kick and blowout occurrences vary from field to field, and have also varied in financial and environmental impact. A survey of 62632 wells drilled in Alberta, Canada over a ten year period from 1979 to 1988 revealed that kicks occurred in 2457 wells. This is approximately 3.9% of wells drilled, from a high of 5.7% for exploratory wells to a low of 3.2% for development wells. Susceptibility to kick was also shown to increase significantly as well depth increases. For wells less than 1000 meters in total depth, the kick rate was 2.3%. This increases dramatically to 54% for wells exceeding 4000 meters [5]. 44.7% of these kicks occurred during drilling operations, 48.5% of kicks occurred during tripping operations, while only 6% of kicks occurred during casing, testing and/or circulating operations. 0.8% of kicks were classified as "other".

22 blowouts occurred over the same period which gives one blowout for every 2850 wells drilled [5]. Twelve of the blowouts were on exploratory wells while ten were on development wells. Another survey for the US Gulf of Mexico showed a much higher blowout rate of one in 162 exploration wells and one in 291 development wells drilled [33]. These significant increases in blowout rate is partially attributable to the inadequacy of kick detection and well control methods in handling more strenuous drilling terrains. While the frequency may seem manageable, the huge financial and

environmental impact of offshore blowouts, sometimes running into billions of dollars, make it impractical to not seek better means of early gas kick detection and control.

2.2 DRILLING AND MUD CIRCULATION EQUIPMENT [29]

The drilling equipment used depends on the type of drilling ongoing at the well site. Classification could be based on various features such as the type of power used, e.g. mechanical, electrical, pneumatic, or hydraulic; the type of pipe used, e.g. conventional, cable or coil tubing; and also the means of rotation or drilling provided for the drill bit, e.g. top drive, rotary table, sonic, or hammer. Our focus is on conventional drilling which involves the use of a drill pipe to advance the drill bit into the rock formation. The derrick is usually vertical in this case and any means of power and rotation could be used alongside. It also employs hydraulic rotary drilling, although a top drive can also be used.

The more visible and common drilling and mud circulation equipment used in conventional drilling include:

2.2.1 The Blowout Preventer (BOP) Stack

The BOP is used primarily to shut in the well i.e. keep reservoir fluid from escaping to the surface while drilling, tripping and well completion is ongoing. It is essentially a large valve installed on the sea floor (subsea BOP) for offshore rigs, or on the wellhead for onshore rigs. They may also be installed below the deck of the rig for offshore wells. It is a high pressure device designed to cope with extreme pressures that may arise when gas kicks go uncontrolled and formation fluid begin to escape to the surface. Additionally, when operating as intended, it is able to contain the drill string, casing, drill bit, mud pump, sensors, drilling fluid and any other equipment or substance still underground, and prevent them from blowing out into the surface under the high pressures that is common during blow outs. Apart from preventing harm to rig

personnel and loss of rig equipment, this sealing in of the wellbore is also necessary to kill the kick through the bypass choke line in order to regain control of the well and subsequently continue drilling. A schematic of a Varco BOP is shown in Figure 2....

2.2.2 Drill Pipe/String

It is a seamless tube that is used to rotate the drill bit in conventional hydraulic rotary drilling, as well as channel the drilling mud to provide hydrostatic balance to reservoir pressure. Drill pipe movement is called tripping. Tripping in involves lowering the drill pipe into the wellbore, while tripping out describes the process of removing the drill pipe from the wellbore. This may occur for various reasons, e.g. bent pipe, blunt bit and faulty mud motor. Drill pipes come in lengths of about 30 thirty feet long and a variety of diameters. They are coupled together at the ends to make up the entire length of the well. The drill collar is attached to the drill pipe holding the drill bit. It provides needed weight on the drill bit as well as housing for the mud circulation pump installed downhole.

2.2.3 The Drill Bit

The drill bit is in direct contact with the formation being drilled and grinds a path through the formation as dictated by the drilling crew. Drill bits are of two main types:

- Fixed cutter drilling bit in which the bit has no moving parts. Cutting action is as a result of the rotation of the drill string.
- roller cone drilling bit which has moving cutting edges.

The selection of appropriate drilling bits depend on the type of formation to be drilled. Formations may be soft, medium or hard. Examples of soft formations include sandstone, clay, soft shale and alluvial beds. Medium formations are lime stones, dolomites and calcites. Soft and medium formations have low compressive strengths

due to the relative "looseness" of the formation particles. Hard formations include hard shale, mudstones and abrasive formations with cherty streaks. Information about the type of formation in an area is abundant well-drilled areas. Very hard materials such as tungsten carbide inserts and polycrystalline diamonds are used to make drill bits. This is to provide resistance to abrasion and bearing wear from the formation, cuttings and the hook load.

2.2.4 Wellbore Casing

These are large diameter hollow pipes of various diameters that are inserted into the drilled open hole to hold the wellbore walls in place. They are inserted in a descending fashion, from larger diameter casings at the top of the wellbore, to smaller diameter casings as the drilling progresses. They are held in place by the drilling cement. Casing lengths vary as determined by the drilling engineer and often depends on formation properties, drilling method employed, and cost considerations. Among other functions, wellbore casings are used to

- Hold the wellbore in place and prevent it from caving in.
- Prevent fluid influx from the formation into the annulus of the wellbore.
- Prevent drilling mud loss into the formation
- Provide a strong upper wellbore to support deeper drilling

The space between the inner casing diameter and the outer diameter of the drill pipe is known as the annulus of the wellbore. The various casing diameters inserted into the wellbore must be large enough to accommodate the diameter of the drill bit to be used for the subsequent well section. Figure 2.... shows a typical casing arrangement.

2.2.5 Mud Pit

These are large storage tanks used to capture the circulating mud from the wellbore and re-circulate it back into the wellbore via a mud pump. Mud pits vary from

rectangular steel tanks of around 200 barrels to mush larger tanks with capacity of up to 1000 barrels. Pits are of two types:

- Single pits, where one mud pit temporarily stores all the drilling mud circulating through the wellbore, and
- Active pits, in which several tanks of varying capacities hold drilling fluids and the sum total is continuously updated in a virtual mud pit totalizer.

Aside from providing a temporary storage for drilling mud, the mud pit also serves as an indicator for gas kicks, provide for the addition of additives to the mud and separation of shale. It typically has various compartments.

2.2.6 Mud Pumps

Mud pumps provide the means of filling the wellbore with drilling mud and maintaining circulation of the mud. They are large reciprocating pumps which are either single acting or double acting. They also provide a means of controlling the flow rate into and out of the wellbore. Mud pump pressure variations are an important gas kick indicator.

2.2.7 Drilling Mud

Drilling mud is used primarily used to provided hydrostatic pressure to balance formation pressure and prevent formation fluids from entering the wellbore while drilling, trilling or during well completions. Drilling muds are of three types:

- Water Based Muds (WBM)
- Oil Based muds (OBM), and
- Gas drilling fluids

Water based muds are primarily composed of water as the continuous phase, with the addition of a percentage of mud solids to give it the required fluid density and other properties. They are relatively cheaper than oil-based muds and are more

compliant with environmental regulations governing the disposal of used muds. Additionally, most gases are almost insoluble in water and hence WBM do not mask gas kicks. It is thus easier to detect gas kicks in WBM than in OBM. However, they suffer many limitations including being unsuitable for drilling in deepwater, high temperature, high pressure zones because of their instability at high temperatures and the tendency to dissociate. Drilling rate is lower in WBM than in OBM, and they tend to cause shale to swell and disperse in water causing clogging of the drilling path.

Oil based muds have oil as the continuous phase. Water and other drilling mud additives make up the dispersed phase. They come in handy in deepwater, high temperature, high pressure drilling, due to their stability at high temperatures. Drilling is able to take place at a high drilling rate, and they do not dissolve shale. Thus clogging is minimized with the use of OBM. Limitations include environmental contamination of freshwater zones encountered while drilling and relatively higher cost of mud.

Gas drilling fluids are applied in reduced -pressure drilling where it is required that the density of the drilling fluid be less than that of water. They range from dry gas, to mists, foams and aerated mud. They find application in drilling of weak formations. In these situations using WBM or OBM could result in lost circulation. Gas drilling fluids also result in high penetration rate due to reduced pressure differential between wellbore bottomhole and the formation. Gas drilling muds suffer the limitation of potential plugging of the annulus when water bearing formations are drilled through.

Apart from stabilizing the wellbore by maintaining a pressure head to balance the formation pressure, the other functions of drilling mud include:

- cleaning of the fluid flow path, i.e. the drillstring and annulus
- transporting and removing cuttings from the wellbore. These are separated in the shale shaker before the cleaned mud is re-circulated

- lubricate and core the drilling bit and underground drilling equipment and sensors
- Transmit hydraulic power to the drilling bit via the mud motor
- Stabilize wellbore during tripping and well completions
- Control corrosion of drillstring and wellbore casing

2.3 MUD LOGGING

This is the process of monitoring the drilling process by keeping detailed records of changes in key indicators of the drilling process. This permits the prediction of potentially dangerous situations like a gas kick or blowout. Mud logging primarily satisfies two basic functions:

- monitor the density of the drilling mud, and
- detect hydrocarbons in the drilling mud and formation cuttings.

While the density of the return mud serves for the prediction of a gas kick or blowout, hydrocarbons in the mud and cuttings give a prediction of reservoir productivity.

Mud logging is done on-site and with computers that track changes of key parameters in real time. These parameters include mud pit gain/loss, return flow rate, inflow rate, pump pressure, stand pipe and annular pressures, gas cut in mud, Rate of Penetration (ROP), etc. These are measured continuously with the help of flow meters, level meters and Measurement While Drilling (MWD) sensors. They are analyzed by the computers and displayed side by side in various real time or delayed charts. If the values of any parameter where to change drastically as to indicate an abnormality, an alarm may be raised to draw attention of the drilling crew. Remedial course of action is then determined if it was decided that an abnormality existed in actual fact.

2.4 CHALLENGES OF DRILLING IN STRENUOUS TERRAINS

2.4.1 Deepwater Drilling

For deepwater drilling, early gas kick detection is very critical. If kicks are allowed to build up beyond a certain amount before well shut-in, it could cause underground blowout of the formation at the casing seat. This maximum amount of kick size that provides for safe shut-in is called the critical kick size. It has been shown that critical kick size is a function of water depth. As water depth increases, critical kick size reduces. Also, the difference between fracture and pore pressure is reduced as water depth increases, making it more difficult to achieve the correct amount of mud weight to balance the pore pressure without exceeding fracture pressure of the reservoir [3].

2.4.2 High Pressure High Temperature Wells (HPHT)

Because HPHT wells are usually slim-hole wells, kick propagation time from formation to the surface is potentially reduced due to reduced wellbore volume [4]. This makes drilling in such wells a delicate balancing act.

2.4.3 Depleted Wells

The main challenge with depleted wells is the narrow geo-pressure margin between fracture pressure and pore pressure (reservoir pressure). This can lead to overbalance, causing lost circulation which may subsequently lead to a kick, blowout or formation fracture and collapse, if uncontrolled. The reason for the narrow pressure differential margin is that depleted well formations are not homogenous [21, 22]. Oftentimes, low permeability shale layers interlay producing zones with higher permeability causing production rates to vary from zone to zone. When depleted, the shale zones continue to retain more fluid and consequently have higher pore pressure than other zones. Pressure difference of several thousand psi have been reported [22]. Also, depletion weakens the formation rocks, resulting in lower fracture pressure. The

higher pore pressure in some zones coupled with lower fracture pressure in the more depleted zones results in a reduction in the margin between pore pressure and fracture pressure for the formation. The challenge while drilling is to balance the pore pressure without exceeding the fracture pressure. Hence special care must be taken in the selection of drilling mud with the right properties to maintain wellbore stability in both static and dynamic modes, and also the drilling technique to be used.

Early gas kick detection could mean the difference between low Non-Productive Time (NPT) and substantial non-productive time - if the kick is eventually controlled - and blowouts, if uncontrolled. The increased incidences of gas kicks and blowouts in these difficult terrains indicate a need for better research on the subject to better understand and model the interactions between wellbore and formation so that prediction and control is more successful. Some current models over-simplify these interactions [2].

2.5 CAUSES OF PRESSURE IMBALANCE

The pressure imbalance that gives rise to gas kicks and lost circulation could result from [2, 8],

i. Too high or too low mud density resulting in wrong hydrostatic bottomhole pressure thereby creating overbalance or underbalance respectively.
ii. Transient effects during pump startup or shutdown. The rapid change in flow rate during this processes result in sudden pressure changes which propagates from the pump to bottomhole at the speed of sound in the mud. These sudden changes in pressure could lead to pressure imbalances at the wellbore-reservoir interface and potentially become a kick initiator.
iii. Drilling through porous rocks or high pressure areas

iv. Low level of fluid in wellbore as a result of drilling maneuvers or lost circulation.

v. Reservoir gas diffusion through mud cake.

The approach to kick control involves kick detection, shutting in the well by means of the blowout preventer (BOP), applying weighted mud through a kill line to stabilize the well and finally, circulating the kick out of the wellbore. Early kick detection typically means detection after about 3 to 5 barrels, or less, of influx [1].

2.6 GAS KICK INDICATORS

Gas kicks are detected by indicators [2, 9] which are divided into primary and secondary kick indicators. Classification may also be made based on whether they occur during a drilling operation or a drilling maneuver such as pipe tripping.

Primary kick indicators provide for easy detection and are dominant in current well crew use for detection, while secondary indicators may also be indicators for other drilling anomalies or drilling maneuvers ongoing at the time.

2.6.1 Primary kick indicators are:

2.6.1.1 Kick Indicators while Drilling

I. Mud Pit Gain [3, 7, 11, 12, 13, 14]: an increase in the volume of mud in the mud tank at a constant inflow rate provides an indication of a gas kick. It involves close monitoring of the fluid volume in the mud pit by the mud engineer as measured by pit level meters. Alarms go off when pit gain exceeds an anticipated, preset level which usually equals the flow-in rate. Mud pits are either single pits - where mud is pumped into the wellbore from a single pit and routed back to the same pit - or active pit, which provides for using different pits for different wellbore fluids but aggregating the separate volumes into a single virtual pit totalizer on a computer screen. They are both easy to monitor. However, single pits are unsuitable where multiple wellbore fluids have to be

used, and active pits have to be closed loop to ensure that monitoring is easy and uncomplicated.

Advantages of using mud pit gain as a kick indicator:

a. Over a long period of time, it provides the most reliable estimate of total kick volume.
b. Measuring/monitoring devices are cheap and easy to install.
c. Because of large pit volumes, noise in readings is less than in other detection mechanisms.

Limitations:

a. Also because of the large pit volumes, it has low sensitivity and accuracy for real time measurements.
b. Detection normally occurs after 5 to 10 barrels of influx
c. Detection is slower than outflow rate indicators. This is because the parameter being measured (volume or height of mud) is an integral of outflow rate, therefore it lags outflow rate.
d. Solubility of gas in Oil Based Muds (OBM) reduces sensitivity and accuracy of measurements.
e. Detection demands continuous fluid flow in the wellbore. If there is low fluid level in the annulus, or no fluid return at the flow meter, detection is impaired.

II. Increase in Outflow Rate [3, 4, 10, 11]: Flow out is measured by a flow meter placed on the return line above the mud line. Measurements are in real time and a comparison is continuously made with the constant inflow rate. Sustained deviations between both quantities provide an indication of gas influx into the annulus or lost circulation into the reservoir. Display of the readings may be in the form of separate displays for inflow and outflow, or a single display of delta flow, given by:

Delta flow = flow out - flow in

Flow out or delta flow exceeding preset limits trigger an alarm as an indication of gas kick. Using delta flow, however, eliminates the need to change flow out limits each time there is a change in flow in rate. Kick detection is faster using outflow rate/delta flow as an indicator than using mud pit gain but measurements tend to be noisy, especially in high heave, deepwater drilling conditions. It also suffers the same limitation as mud pit gain when there is no fluid return at the flow meter.

2.6.1.2 Kick Indicators while Tripping [34, 35]

III. Incorrect fluid fill while tripping out: this normally occurs if there is a gas kick event during tripping in or out. It does not apply while actual drilling is ongoing. Tripping involves pipe movement in or out of the wellbore and occurs when drill bits wear out or when downhole sensors require maintenance or replacement. During this period drilling is suspended. Simultaneous fluid filling of the wellbore while tripping out is important and necessary in order to maintain the bottomhole pressure and prevent an underbalanced situation. If there is excess pit gain while tripping in or a deviation from what is theoretically required to fill up wellbore while tripping out, a kick may be occurring.

IV. Positive flow: during tripping, if the pumps are turned off when the drill pipe is stationary, and a manual flow check on the return line confirms an outflow, this could be an indication of a kick.

2.6.2 Secondary kick indicators are (14):

I. Decrease in standpipe pressure: when gas enters the annulus of the wellbore, the density of the annulus fluid decreases. This reduces the hydrostatic pressure in the annulus at the bottomhole. The fluid in the drill string maintains its

pressure and pressure potential is created forcing more fluid from the drill string into the annulus thereby reducing the drill pipe pressure.

II. Increase in rate of penetration, also called drilling break, occur as a result of the bit encountering a more porous formation than it previously drilled through. While this may not necessarily lead to a kick, vigilance is required since a new formation with different properties may mean an impending pressure imbalance.

III. Increase in gas cut: an increase in the amount of gas in the return mud, measured at the mud pit, may be an indication of a gas kick.

2.7 KICK DETECTION METHODOLOGIES

The history and methodology of gas kick and lost circulation detection has followed from using these indicators to trigger alarms when detection occurs and kicks reach preset values, and also to quantify the amount of kicks in order to facilitate well shut in and accurate well control. The challenge has always been to detect kicks early on so as to reduce NPT and mitigate the risk of blowout. More recently, downhole measurements of drill pipe and annulus pressure, among others, are being explored for improved monitoring of kick detection. The aim of the differing methodologies has been to detect kicks as early as possible.

Literature review suggests that the closer the location of real time measurement to the formation, the earlier the kick would be detected [8].

It is widely accepted in drilling literature that flow out minus flow in (or delta flow) provides for more rapid kick detection than mud pit gain [10]. Both of these involve surface measurements. For each of these indicators, differing methodologies and physical principles are used. Kick detection success is measured by how early kicks

are detected, absence or low number of false alarms, ease of installation of equipment, and cost [4, 11].

This review follows the development of these methodologies as broadly categorized under three early kick detection indicators: mud pit gain, outflow rate and downhole measurements. It provides the state of the art at the present time.

2.7.1 Detection using Mud Pit Monitoring [11]

Mud pit gain is one of the earliest indicators of gas kick used in the industry and is the simplest and most widely used method in the late 1980s [12]. Detection only after eight to ten barrels change in pit volume is considered normal but recent advances in technology has improved this figure to about five barrels of influx into the wellbore [13].

Measurement is usually done with meters that range in complexity from the simple float meter to more modern ultrasound meters. Readings are relayed in real time to the drilling monitoring station. When the height of mud in the tank exceeds a preset value, an alarm is raised and the next course of action is determined by the drilling crew. Because of large tank volumes, sometimes as large as 200 barrels, sensitivity and accuracy is a problem in using mud pit gain as a kick indicator. Ultrasound meters provide for greater sensitivity and accuracy, but they come with expensive price tags. The use of more complex mechanisms and algorithms to couple mud pit gain as a kick indicator has been to increase sensitivity and accuracy especially in high heave, deepwater drilling.

The type of mud used also affects response time. Oil Based Muds (OBM) have high gas solubility especially at high pressures. This has the effect of inhibiting gas kick detection until after a substantial volume of gas has entered the wellbore. Water Based Muds (WBM) do not have this problem, hence WBM has a better response time when compared to OBM. However, for deepwater, HPHT, and wells with chemically related

wellbore instability, OBM is preferred to WBM [13] because it is chemically stable and does not dissociate in high temperature environments. It also serves as a lubricant, thereby reducing drilling torque. A limitation of OBM is that they are not environmentally friendly. However, if treated and re-used, this limitation is mitigated.

Artificial Neural Networks (ANN): Mud pit gain is used as a kick detector in these networks. They are information processing systems inspired by the way biological nervous systems process information [14]. ANN are non-algorithmic, distributive, analog and parallel information processing methods capable of discovering complex relationships between variables presented in the network, and also map input to output no matter how complex the relationship [15]. They consist of three layers: input, hidden, and output layers. They are classified as dynamic and static networks. The latter uses current input to model current output, while the former uses current and previous inputs, and sometimes previous output to simulate current output. These networks are capable of "learning" and are "trained" using input data to discover the complex relationships among variables in the network through a feed forward process.

For kick and loss prediction, variables include drilled depth, Rate of Penetration (ROP), pit volume, pump pressure, flow in rate, and mud weight, among others [14]. When changes in these variables exceed preset thresholds as would indicate possible kick or lost circulation, an alarm is triggered. Pit volume provided the best measure of kick, giving the highest detection rate with a corresponding lowest number of false alarms.

This technique, much like other engineering techniques inspired by biological processes e.g. Genetic Algorithms, has the potential for versatility and application to all drilling terrains since it requires training the network and setting sensitivity as needed. The technique already finds application in engineering systems and processes, airport security and the financial industry [15]. The method also provides greater reliability than flow out or delta flow methods, as noise in pit volume proves to be less than in flow out

measurements. Detection thresholds could also be set and adjusted as required. A limitation is susceptibility to poor sensitivity and high number of false alarms. Detection time has an inverse relationship to false alarm rate. Both are dependent on the kick probability threshold. Decreasing the threshold will decrease detection time but increase false alarm incidents. This could create a trust problem with the drilling crew [14].

2.7.2 FLOW-OUT RATE

In the absence of gas kick measurement from downhole sensors, outflow rate provides the fastest means of kick and lost circulation detection while drilling [3, 10]. From a positional standpoint, this is expected since it is measured on the return line before fluid gets to the mud pit. But these measurements suffer from accuracy, reliability and noise when compared to mud pit gain [4, 11], especially in high heave conditions. Consequently, it is more prone to raising false alarms and over time, may present a trust issue with the drilling crew. . An additional complication is faced when the output flow meter is not placed so that it can account for the entire outflow from the well. For instance, if some of the flow is diverted to the sea before the flow meter, it can be very difficult (without an additional flow meter for summing total annulus outflow) to calibrate for an unknown kick or loss of circulation material. We'll assume here that the Flow-out rate is all of the material from the annulus.

Outflow measurements are carried out using flow meters on the mud return line. It is done in real time and provides a means of kick or lost circulation determination based on deviation from expected values - the difference between inflow and outflow rate, known as delta flow. In current drilling systems, when delta flow exceeds a set limit, an alarm is raised. The delta flow approach provides an added advantage in that changes in the steady state inflow rate would not require continually resetting alarm levels as would be required with systems using only outflow rate [10].

Many different types of flow meters are used today for outflow measurements [11]. Each has its own advantages and limitations, and whether used alone or in some other fashion as described in more detail below, flow out has proven to be a fast means of detection and control of kick and lost circulation.

Wave propagation technology is used in measurement and determination of gas kicks. The underlying principle is that acoustic wave propagation time varies in different media as it is a function of fluid density and compressibility. This is especially true with two phase systems [16]. When gas is present in liquid, the velocity is substantially reduced. At atmospheric conditions, sound wave will be reduced from 1500m/s to 50m/s, a 97% decrease, if 2-3% gas was mixed with water. Because of gas compression downhole, this effect will be less, but still substantial. Experiments show a 30% decrease in sound velocity at pressures of 4500 psi for 2% gas mix [17].

The Gas Kick Warner (GKW) [17] uses this sound wave propagation principle. A pressure pulse is generated at the standpipe and its propagation time is measured as it travels down the drill string, through the bit, and up the annulus where it is detected at the top. Flow rate wave propagation operates on the same principle. In this case, pressure fluctuations from the mud pump are used as wave sources [16]. Measurements from the pressure transducers at the standpipe and on the return flow line are compared to modeled expectations and deviations beyond set thresholds will activate alarms.

Some flow meters like the ultrasonic flow meter [7, 11] also use the same principle. Ultrasonic level sensors and velocity probes incident on the flowing fluid measure level and fluid velocity from which area and mean velocity is calculated. Volumetric flow rate is calculated at flow in and flow-out and gives an indication of any volumetric gain as a result of gas influx. While it is simple in operation and easy to install, these systems are not suitable for OBM as they are limited to the detection of

free gas. They are also susceptible to interference from Measurement While Drilling (MWD) signals and vibration frequencies of drill bit and drill pipe. Such signal distortion could impair accuracy of results with the attendant delay in detection time or triggering of false alarms. The principle also depends on fluid flow continuity. Hence when making connections or while tripping without pumping, the gas kick detection system is inactive. Signal strength reliability is also an issue.

Acoustic technology is also used for wells experiencing severe lost circulation [18]. Most kick and lost circulation detection methods rely on the ability to measure fluid return at the surface using flow meters or level detectors in the mud pit. In a case of lost circulation where there is no fluid return, the drilling crew would have no indication of kicks while tripping unless the kick builds up or mud is being unloaded from the well. With this technique, an acoustic device is installed on the casing valve to continuously monitor liquid level in the annulus of wells. It operates without the requirement of fluid circulation or that the annulus be full of drilling fluid. Pressure pulses are generated at the surface and directed down the wellbore and the echoes from the collars are recorded when the pulses resurface. The travel time of the pulses give an indication of the fluid level in the annulus. During tripping for example, a rise in the fluid level could be interpreted as an indication of a kick. Also, the correct volume of fluid to pump in while tripping out can be determined [18].

Bayesian probabilistic framework is another gas kick detection methodology based on flow-out measurements [4]. This method is suitable for deepwater drilling under high heave conditions where data can be very noisy. Kicks of various types are modeled exclusively as a time series of flow data. Other signature drilling events that affect outflow and may be mistaken as kicks are also modeled. No thresholds are involved. Hence, two model sets exist. The first is a model set for signature drilling events such as steady state, kick, lost circulation, pipe movement, pump on, and pump off, and the second is a Bayesian probabilistic model matching framework. The former

models incorporate known information about the nature of drilling events and the Bayesian framework compares these models to drilling data on a continuous basis to determine which of the models most closely match current data. It does this by determining relative probabilities of multiple hypotheses, in this case, different rig events. If data suggests a normal rig event occurrence, no alarm is raised. If there is a high kick probability, an alarm is raised.

This kick detection methodology improves sensitivity to less than one barrel in low to medium noise levels with a low false alarm rate [4]. Sensitivity adjustment is automatic and adjusts to the level of noise present in the data. Hence no calibration or sensitivity adjustment is required. It also outputs a measure of confidence in its calculations so the operator can make better judgment as to what action is required. Another advantage is that it requires no additional equipment aside the Bayesian framework console. Normal rig flow meters are used.

Microflux Control (MFC) Equipment [13] is used to mitigate the issue of solubility and response time in OBM. This is a variant of Managed Pressure Drilling (MPD). The method is based on early detection of a minimum kick or loss of fluids and instant adjustment of the return flow, and consequently, the Bottom Hole Pressure (BHP), to regain control of the well. A rotating control device is employed to keep the well closed at all times and divert return flow to a choke. A flow meter determines return flow rate. The return flow is compared with predicted flow, and any discrepancy is compensated for by adjusting the choke. Flow is thereby returned to predicted levels. Control is automated, but can be manual as well [19].

To facilitate instant well control, it is required that fluid in the well bore annulus be incompressible. This is because response downhole for any action at the choke is faster (at the speed of sound of the fluid system) when annulus fluid is incompressible [19]. This creates a disadvantage with the use of OBM because gas is soluble in OBM

especially at high pressures, whereas gas solubility in WBM is negligible. Dissolved gas in OBM makes it more compressible than it would normally be, thereby simultaneously masking gas influx and delaying response time when action is initiated at the choke [12, 13]. Density trending along the annulus differentiates between gas influx and gas expansion.

The advantage of Microflux Control (MFC) is that it has very good sensitivity, usually in the range of 0.25 to 0.5 barrels. At such low levels of detection there is no noticeable difference between response time of OBM and WBM [13] since there isn't enough gas in the system to greatly affect compressibility. MFC saves time by cutting out NPT since well shut-in is not required for well control. BHP correction is also automatic and kick and loss detection is accurate and at minute levels [19]. Limitations include the need for additional equipment and the difficulty in set-up. Also, for gas kicks, the presence of gas in the annulus, no matter how little, potentially increases the response time to balancing BHP when compared to lost circulation. Depending on the amount of gas influx, control may prove difficult and could lead to prolonged wellbore instability with its attendant problems.

2.7.3 DOWNHOLE MEASUREMENTS

Downhole measurements transmitted in real time provide an inherently faster means of detecting kicks and lost circulation than surface measurements. As mentioned previously, our baseline approach will not assume access to these measurements, based on guidance from BP “see if the method can work without these measurements”. However, we include them here, as they represent current state of the art, and potential enhancements for the technique as needed to show distinguishing utility in the field.

Wired drill pipe telemetry involves using measurements from distributed pressure sensors along the drill string is combined with real time analysis of drilling data

to provide valuable information to control the drilling process [8]. Data from the sensors inform a comparison with characteristic pressure curves for normal and abnormal drilling events to predict occurrence or absence of kicks. This holds the potential to estimate the depth of an influx zone as well as kick size by placing the pressure sensors at node points that divide the annulus into control volumes. Real time measurement occurs throughout the drilling cycle and any unexpected changes in flow rate and density measurements within one control volume should induce pressure variations at the nodes. With prior knowledge of the position of each node, accurate information concerning the location and size of kick volume can be determined.

This technique is suitable to vertical deepwater wells and drilling in depleted reservoirs which involve narrow pressure margins between pore and fracture pressures. Pressure changes downhole are detected in real time, and if they indicate a kick, remedial action can be taken quickly. It is also potentially faster than techniques involving surface measurement of mud pit gain and outflow rate.

However, it is unsuitable for horizontal drilling and for well inclinations less than 60 degrees since pressure sensors depend on discernible fluid head. The hydrostatic pressure changes due to gas migration in such situations become too small to differentiate. Pump rate also have to remain unchanged while estimating depth of influx zone and kick volume. If combined with the Bayesian framework earlier described, the technique holds promise for faster detection and versatility.

2.8 OBJECTIVES OF THE RESEARCH

As can be seen in this review, early gas kick detection has become a critical factor in hydrocarbon exploration and development. It has evolved from detection at the mud pit to the return flow line through flow meters, to downhole sensors. The aim is the earliest detection possible so as to make control easier and surer. Mud pit gain provides a veritable measure of overall gas kick or lost circulation volume over time, but detection

time is slow. While outflow (or delta flow) measurements may be noisy especially in high heave conditions, they give a faster, real time indication of gas kick and lost circulation than mud pit gain. Downhole pressure sensors potentially provide the fastest means of detection since they are positioned closest to the formation from where gas influx or fluid loss occurs, relative to the earlier two methods. However, these sensors do not operate well in horizontal wells because of their partial dependence on fluid heads to function as desired.

Modeling the complex interactions between wellbore and formation presents a constant challenge to researchers. These models have also evolved over the decades from the over-simplified models to the more advanced ones of late. Researchers have argued that the aim of these models is to identify a trend, not necessarily to predict exact outcome. This may be true, but the more accurately the interactions are modeled, the better the predictive models become. Real time data are more easily matched to models [20] and detection time and uncertainty is reduced. Overly simplified models may lead to erroneous predictions [2].

Drilling in deepwater, HPHT, and depleted wells have peculiar challenges and early kick detection is crucial to the success of these costly operations. In HPHT for example, kick propagation time is very fast because of the reduced wellbore volume. This makes every second critical.

Our research aims to combine the underlying principles of detection closer to the formation, better modeling of wellbore-formation flow interactions for a wider range of rig operations, and the use of relative probabilities to determine normal or abnormal trends in real time. This provides an opportunity to develop a faster, more accurate, more reliable, sensitive and versatile early kick detection methodology for the more high risk drilling terrains identified above. Our aim is also to eventually go a step further and predict the amount of reservoir influx in real time. This will go a long way in aiding

judgment by the drilling crew on how to go about well control and how much time they have before the situation escalates.

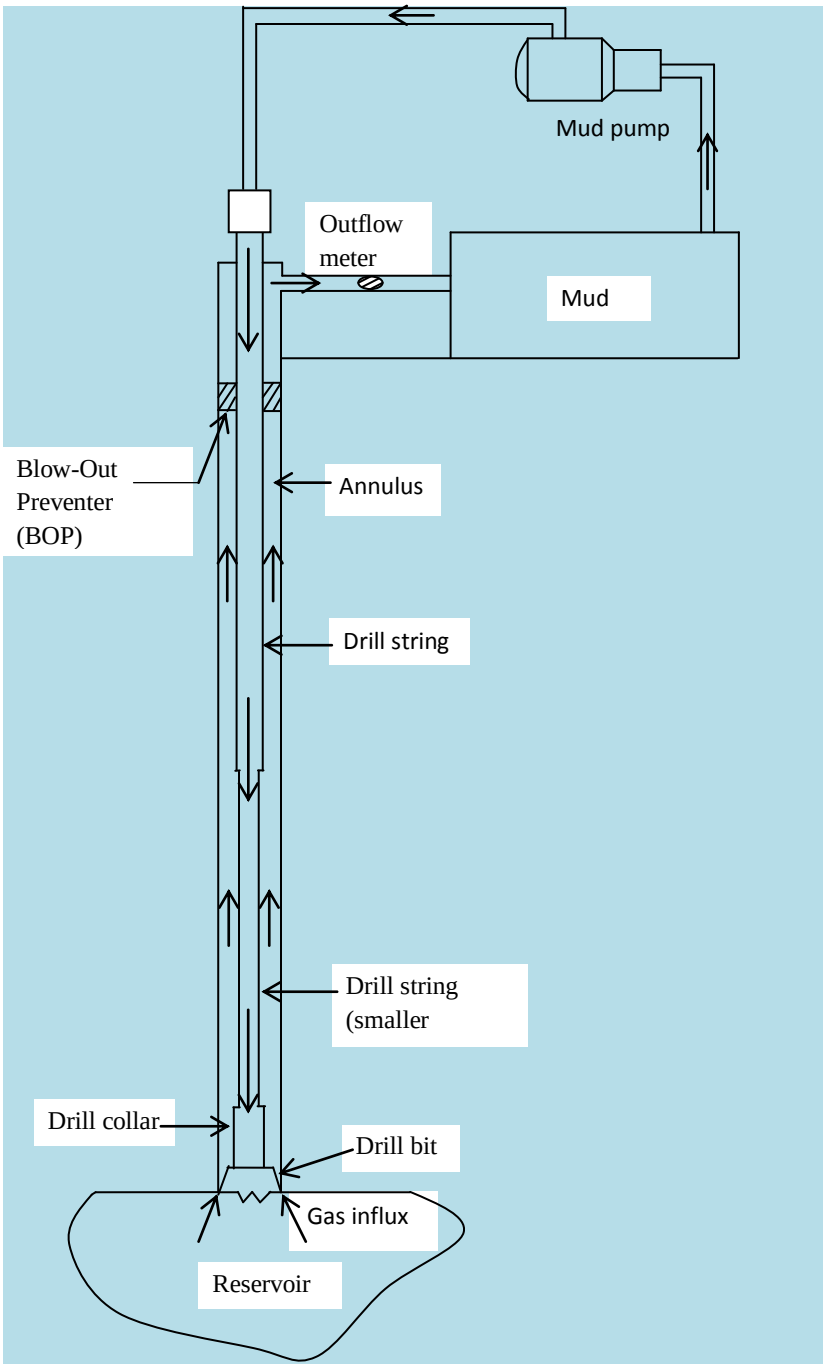

Figure 2.1 Schematic of relative positions of wellbore, reservoir and drilling equipment during a drilling Operation.

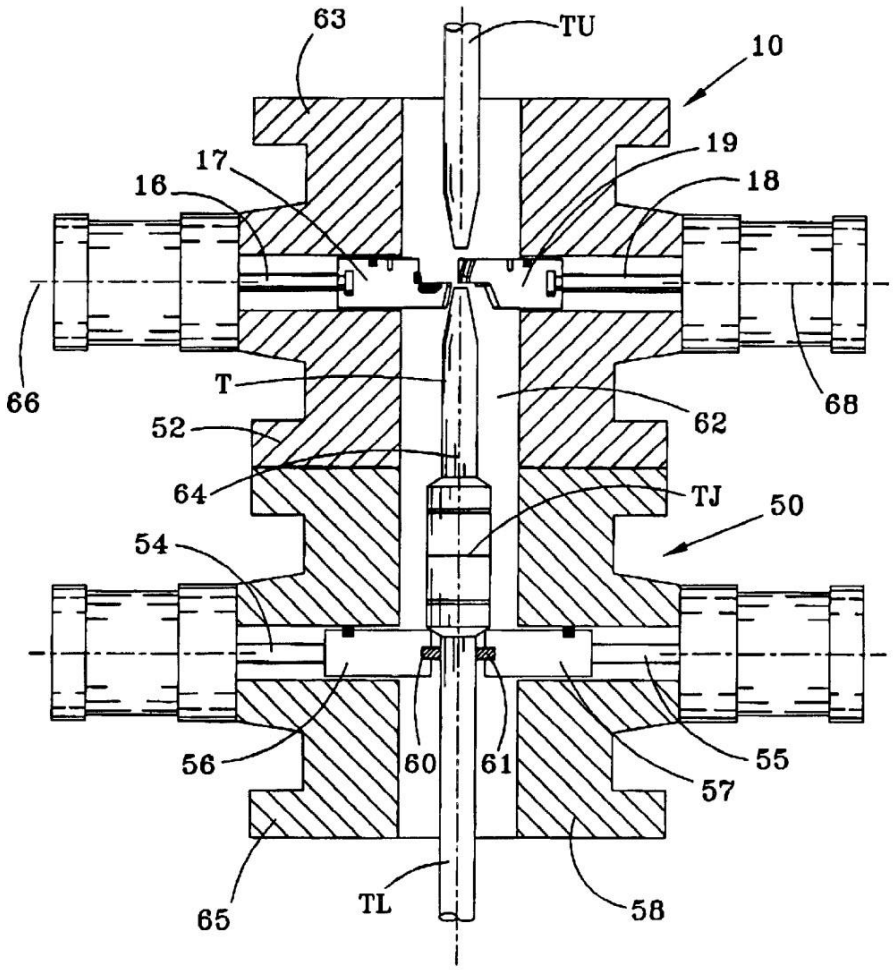

10 Shear Ram Preventer	55 Pipe Ram Shaft	64 Wellbore Axis
16 Shear Ram Shaft	56 Pipe Ram (Ram Block)	65 Lower Flange
17 Lower Blade Shear Ram	57 Pipe Ram (Ram Block)	66 Ram Axis
18 Shear Ram Shaft	58 Housing (Body)	68 Ram Axis
19 Upper Blade Shear Ram	60 Packer (Ram Seal)	T Tubular
50 Pipe Ram Preventer	61 Packer (Ram Seal)	TJ Tool Joint
52 Housing (Body)	62 Wellbore	TL Lower Tubular
54 Pipe Ram Shaft	63 Upper Flange	TU Upper Tubular

Fig 2.2 Varco Schaffer Ram Type Blow-Out Preventer (BOP) Stack

Figure 2.3 A Typical Oil Drilling Bit

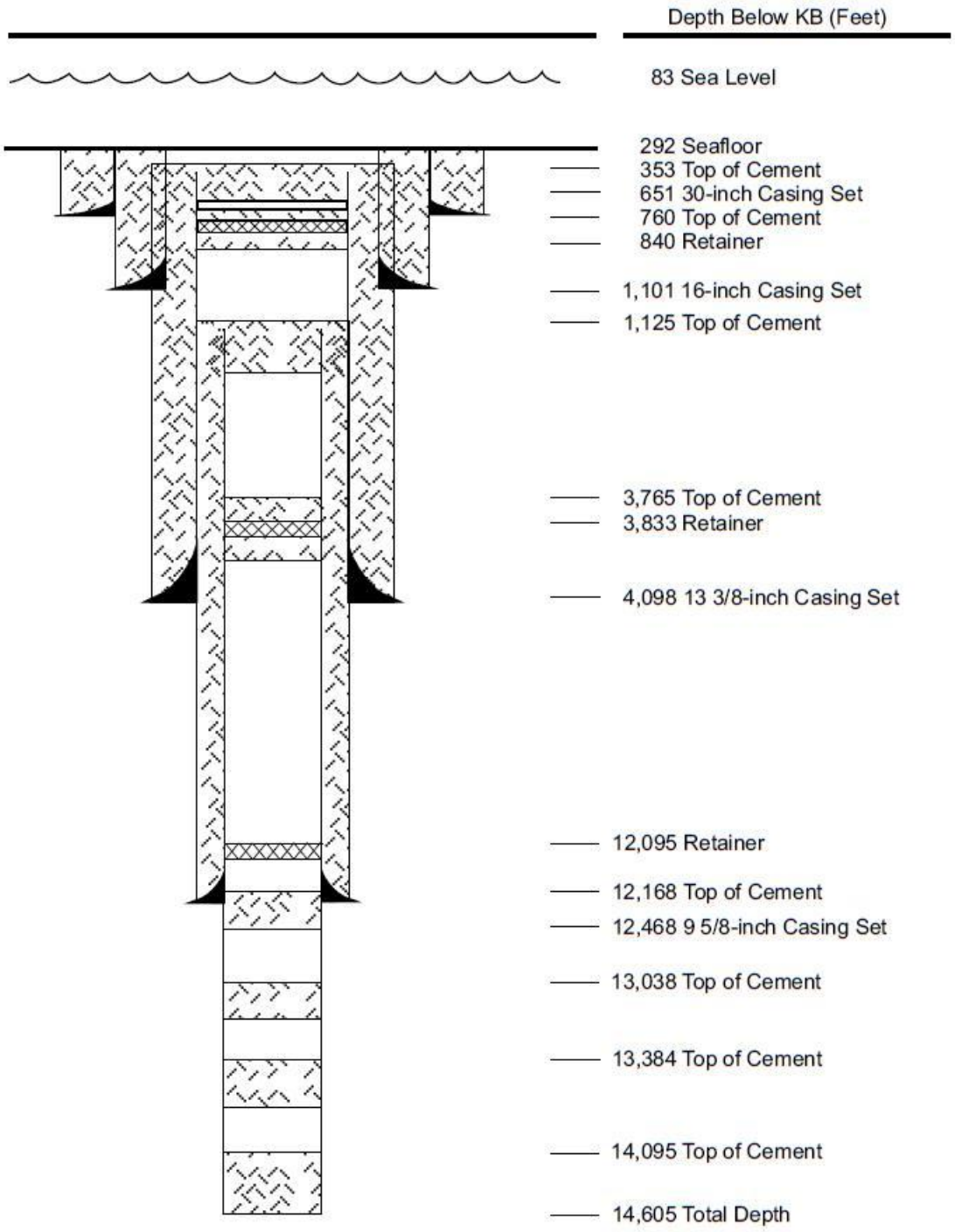

Figure 2.4 Well Casing

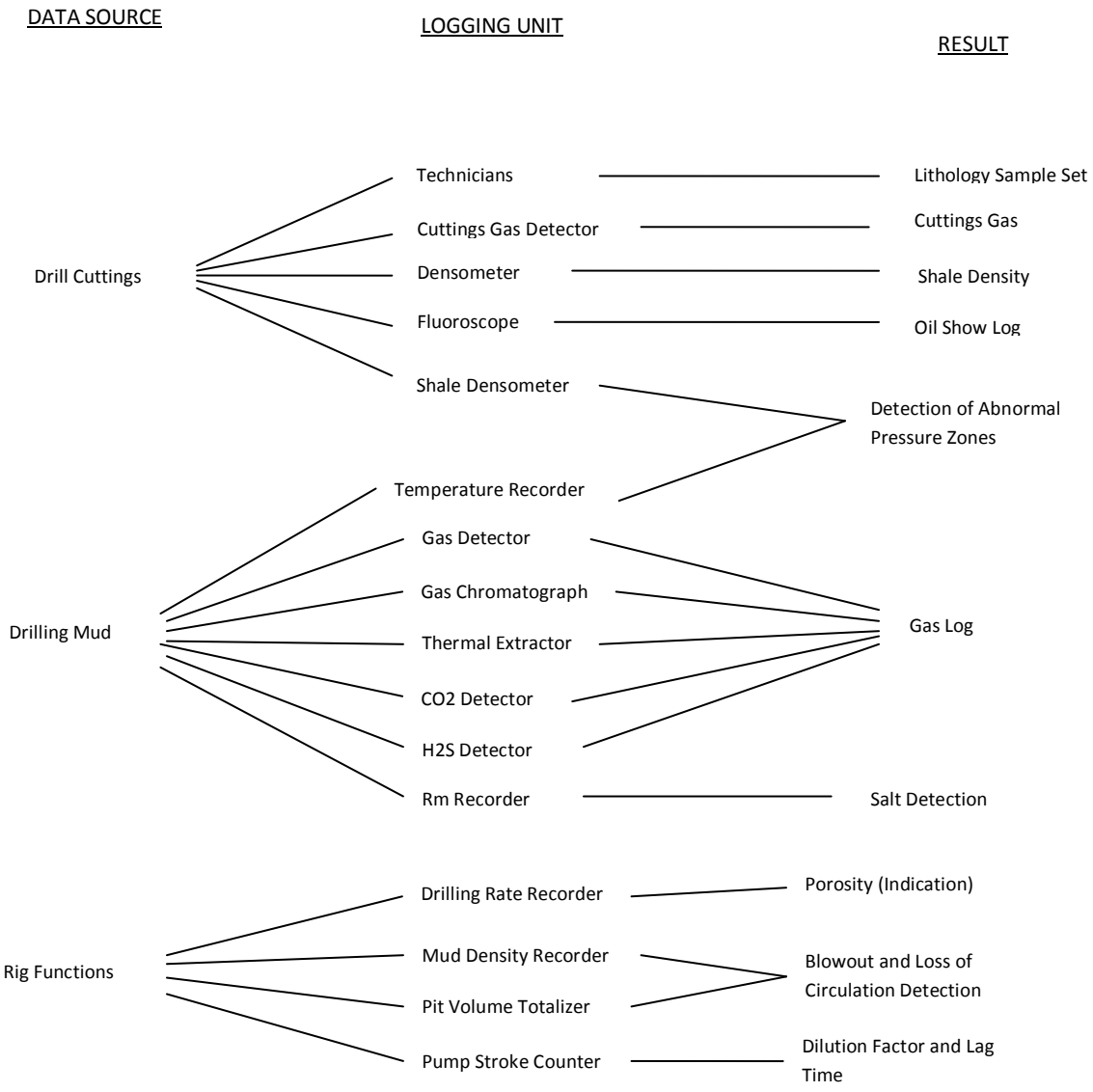

Figure 2.5 Mud Logging Operations [9]

Chapter 3: Early Gas Kick Detection Water-Based Mud Model

Inherent in a model based approach is the assumption that all computational parameters and variables, whether surface or downhole, can be transferred in real-time to calculation servers and that results from the computer models are immediately available for application [23]. The equations developed model the transient hydraulics and well-formation interactions in multiphase flow. The drill string and annulus will be spatially discretized and balance relations and closure equations are defined for each discreet space.

3.1 PHYSICAL EFFECTS ESTIMATED IN THE MODEL

The physical effects estimated in the model are [2]

- Frictional pressure loss, both for single and two phase flows
- Pressure loss in bit
- Pressure loss in choke (if choke is included)
- Viscosity variations with pressure, temperature and composition of the mud
- Density variations with pressure, temperature and gas content of the mud
- Rise in gas velocity as it expands up the annulus
- Simple reservoir dynamics including permeability and porosity of reservoir (when a reservoir model is included).

3.2 MODEL ASSUMPTIONS

The model assumptions are:

- All variables are dependent on only one spatial coordinate - length along flow line. Effects from cross-sectional, non-uniform velocity and mass distribution profiles currently are neglected.

- Temperature at each point along the flow line is known (this is an input to the model based on estimates or measurements made elsewhere)
- Gas in the flow line can exist either as free gas or dissolved gas.
- Gas and mud pressures at the same point are assumed to be equal.
- Gas is insoluble in Water-Based Mud
- System is treated as a black oil system, one that is able to predict compressibility and mass transfer effects between phases in a reservoir as it is depleted.
- The wellbore annulus is concentric

3.3 CONSERVATION EQUATIONS FOR SINGLE AND TWO PHASES

3.3.1 Basic Equations for Single Phase Water-Based Muds

3.3.1.1 Mass conservation of Mud

This is defined as:

$$Mass\ storage + (Mass\ in - Mass\ out) \pm Source/Sink = 0$$

$$\frac{\partial}{\partial t}(A\rho_m) + \frac{\partial}{\partial s}(A\rho_m\, v_m) = 0 \qquad (1)$$

Each of the terms in the equation has units of mass flow rate per unit length.

3.3.1.2 Conservation of momentum

This is defined as:

$$Momentum\ storage + (Momentum\ in - Momentum\ out) + Forces = 0$$

$$\frac{\partial}{\partial t}(\rho_m v_m) + \frac{\partial}{\partial s}(\rho_m v_m^2) + \frac{\partial P}{\partial s} + F - \rho_m g cos\theta = 0 \qquad (2)$$

This results in two equations with four unknowns. To find the unknowns two more equations are needed. These are derived from state equations and correlations relating

the parameters and variables contained in the equations. These will be discussed in section 3.4 that discusses the sub-models for two-phase flows.

3.3.2 Basic Equations for Two-Phase WBM

3.3.2.1 Mass conservation of Mud

This is defined as:

$$Mass\ storage + (Mass\ in - Mass\ out) \pm Source/Sink = 0$$

$$\frac{\partial}{\partial t}(A(1-\alpha)\rho_m) + \frac{\partial}{\partial s}(A(1-\alpha)\rho_m\, v_m) = 0 \quad (3)$$

3.3.2.2 Mass conservation of Gas

This is defined similarly as:

$$Mass\ storage + (Mass\ in - Mass\ out) \pm Source/Sink = 0$$

$$\frac{\partial}{\partial t}\left(A\alpha\rho_g\right) + \frac{\partial}{\partial s}\left(A\alpha\rho_g v_g\right) = 0 \quad (4)$$

3.3.2.3 Conservation of total momentum

This is defined as:

$$Momentum\ storage + (Momentum\ in - Momentum\ out) + Forces = 0$$

$$\frac{\partial}{\partial t}\left((1-\alpha)\rho_m v_m + \alpha\rho_g v_g\right) + \frac{\partial}{\partial s}\left((1-\alpha)\rho_m v_m^2 + \alpha\rho_g v_g^2\right) + \frac{\partial P}{\partial s} + F - \left((1-\alpha)\rho_m + \alpha\rho_g\right) g\cos\theta = 0 \quad (5)$$

This culminates in three equations with seven unknowns. To find the unknowns, four more equations are needed. These sub-models, derived from state equations,

correlations and established relationships between variables, provide the closure equations. They are:

i. Gas density: $\rho_g = \rho_g(P,T)$ (6)

ii. Mud density: $\rho_m = \rho_m(P,T)$ (7)

iii. Free gas velocity: $v_g = v_g(P,T,\alpha,s,v_m,v_{gs})$ (8)

iv. Frictional pressure loss: $F = F(P,T,\alpha,s,v_m,v_{gs})$ (9)

3.4 DETAILED DESCRIPTION OF SUB-MODELS

3.4.1 Gas density:

$\rho_g = \rho_g(P,T).$ (10)

This is found from the real gas law:

$\rho_g = \frac{PM}{RTz}$ (11)

$M = \delta_g M_a \quad ; \quad M_a = molecular\ mass\ of\ air = 29\frac{lbm}{lbmole};\ R = 10.73\frac{psia(ft^3)}{lbmole(R)}$

$=> \rho_g = 2.7\frac{\delta_g P}{Tz}$ (12)

$=> \rho_g = KP$ (13)

Where,

$$K = 2.7\frac{\delta_g}{Tz} \quad (14)$$

P and T are pressure and temperature at each spatial coordinate. The modified Redlich-Kwong equation of state (EOS) is also used in some models [22].

3.4.2 Mud density

$$\rho_m = \rho_m(P,T) \quad (15)$$

Mud density is calculated by adjusting surface mud density to take into consideration the compressibility of liquid phase. For WBM, water density, ρ_m, is found at varying P and T using correlations for slightly compressible fluids such as water [28].

$$\rho_m = \rho_{lsc}[1 + c_l(P - P_{sc}) - c_{Tl}(T - T_{sc})] \quad (16)$$

$$=> \rho_m = \rho_{lsc}[1 + c_l(P - P_{sc}) - c_{Tl}(T - T_{sc})] \,.\, {}^{P}/_{P}$$

$$=> \rho_m = \phi P \quad (17)$$

Where,

$$\phi = \rho_{lsc}[1 + c_l(P - P_{sc}) - c_{Tl}(T - T_{sc})] \,.\, {}^{1}/_{P} \quad (18)$$

Mud solids are incompressible. The density of the gas/liquid mixture is

$$\rho_{mix} = \rho_g\alpha + \rho_m(1-\alpha) \quad (19)$$

$$\rho_{mix} = KP\alpha + \phi P(1-\alpha) = P(\phi + K\alpha - \phi\alpha) \quad (20)$$

3.4.3 Free gas velocity:

$$v_g = v_g(P, T, n, x, \alpha, s, v_m, v_s) \text{ [22, 25]} \quad (21)$$

This is obtained from an empirical correlation, and is a sum of the average mixture velocity, v_{mix}, and the relative slip velocity, v_{gs}. The relative slip velocity is the relative motion of the gas with respect to the average velocity of the gas/liquid mixture [22].

$$v_g = v_{mix} + v_{gs} \quad (22)$$

$$v_{mix} = K_g[v_m(1-\alpha) + v_g\alpha] \quad (23)$$

$$\Rightarrow v_{mix} = K_g v_m(1-\alpha) + K_g v_g \alpha \quad (24)$$

Putting (24) into (22),

$$v_g = K_g v_m(1-\alpha) + K_g v_g \alpha + v_{gs} \quad (25)$$

$$\Rightarrow v_g(1-K_g\alpha) = K_g v_m(1-\alpha) + v_{gs}$$

$$\Rightarrow v_g = [K_g v_m(1-\alpha) + v_{gs}]/(1-K_g\alpha)$$

If $K_g = 1$, then

$$\Rightarrow v_g = v_m + \frac{v_{gs}}{(1-\alpha)} \quad (26)$$

$$v_{gs} = v_{gs}(\rho_g, \rho_m, \alpha, \sigma, d_e, d_i) \quad (27)$$

The relative slip velocity is a very important factor in gas kick analysis and modeling, and an accurate and realistic model cannot be achieved without including this phenomenon [22]. It captures fluid interactions as gas enters the wellbore and expands on its way up the annulus. It is a function of gas and liquid phase properties as well as the amount and distribution of the gas in the annulus. Some existing models either completely ignore relative slip or use simplified assumptions [22].

3.4.3.1 Two Phase Flows

Two phase flows result in mud and gas distributions that create several observable patterns or flow regimes that describe the degree of separation of the two phases. The type of flow regime vary from point to point along the vertical wellbore depending on the phase properties, relative velocities of the mud and gas, and the void fraction or liquid hold up of the gas and mud phases respectively [22, 29]. It is also determined by [34, page 173]

- A balance between fluid mechanical properties that enhance dispersion (turbulence in the continuous phase) and those that enhance separation (density difference being the driver here)
- Initial condition of the multiphase flow
- A mixture of both effects

The two ends of the spectrum are dispersed flow and separated flow. Dispersed flow is sometimes assumed as homogenous or single phase flow because the dispersed phase is widely distributed as infinitesimally small bubbles or particles in the continuous phase. Separated flows involve separate parallel streams of the phases. Between these two limits, there are varying degrees of separation in the flow, and this determines important characteristics of the flow. Figures 3.1 and 3.2 show flow regime maps using

gas and liquid momentum fluxes and gas and liquid volumetric fluxes respectively. The flow is for an air/water mixture in a vertical pipe.

The prediction or determination of the type of flow regime present at any node point is important in accurately evaluating the slip velocity and friction pressure losses in the flow. This is analogous to the determination of whether flow is laminar, turbulent or transition in single phase flows so as to determine the friction factor. Our interest is in vertical flows which have slightly different observable flow patterns to those found in horizontal flows.

3.4.3.2 Flow Regimes in Vertical Flow

Two phase upward flow of mud and gas results in several distributions of the phases in the mixture. These are shown in Figure 3.3 described below:

I. Bubble Flow

The gas phase is dispersed in the continuous mud phase as an infinite number of very small bubbles. The size and shape of the bubbles may vary but they are typically almost spherical in shape and the particle size is much smaller than the pipe diameter. This is termed homogenous multi-phase flow [34, page 173]. This implies that there is no relative motion. However, this is an erroneous assumption as there many cases of dispersed flow involving very small gas particle sizes but in which significant relative motion exist between the phases. Bubble flows occur at very high flow rates, as typically exist at the bottomhole of the wellbore or at points of influx of the gas phase into the continuous mud phase.

II. Slug Flow

As the gas void fraction increases, small bubbles collide and coalesce to form larger bubbles. This process continues until the dimensions of the bubbles grow to become similar to the tube diameter. Slug flow bubbles have a characteristic

hemispherical nose and a blunt rear end. They are usually separated by slugs of liquid. The bubbles are commonly referred to as Taylor bubbles because of their unstable nature [35, chapter 12-1].

Slug flow is one of the few different gradations of separated flows that include Churn flow, Annular flow, and Annular Mist/Dispersed flow. These have varying characteristics, shape and size depending on the void fraction, the velocity of the moving particles, inclination of the pipe, and the size and distribution of the gas phase. They are usually characterized by a film of liquid on the walls and a central core of gas separated by liquid films or slugs, which may include entrained gas dispersed as small bubbles within them. See Figure 3.4

The slip velocity of bubble and slug flows are given by equations, the selection of which is determined by the void fraction of the gas as depicted in Figure 3.5. Between these two ends, flow is designated as transition flow. In determining the friction factor however, four classifications are used, thus: distributed (bubble) flow, segregated (slug) flow, transition flow and intermittent flow. These classifications are determined both by the void/liquid fractions, as well as correlations developed by the researchers.

It should be noted that these correlations are used to provide results that more accurately reflect experimental results, and this may be different from one researcher to the next.

Relative slip between phases is given by formulations that describe one of three approximated flow regimes [2, 22]: bubble flow, fully developed slug flow, and transition flow.

The average bubble slip velocity is given by

$$v_{gs} = 1.41[\rho_m^2 \sigma g/(\rho_m - \rho_g)]^{1/4}, \quad 0 < \alpha < \alpha_b \tag{28}$$

Substituting equations (9) and (12) into equation (18), we have

$$v_{gs} = 1.41[(\phi P)^2 \sigma g/(\phi P - KP)]^{1/4},$$

$$=> v_{gs} = 1.41[P\sigma g\phi^2/(\phi - K)]^{1/4}, \quad 0 < \alpha < \alpha_b \qquad (29)$$

where α_b is a maximum value below which bubble flow is assumed to exist. α_b may be as high as 0.5 for highly turbulent flow in vertical pipes but is usually in the range of 0.25 [22]. When the void fraction,α, exceeds that of a fully developed steady-state slug at the same pressure, temperature and geometry, slug flow is assumed to exist. This occurs at values of $\alpha_{sl} \geq 0.85$. The relative slip for a slug flow regime is given by:

$$v_{gs} = 0.55K_g[(d_e + d_i)(\rho_m - \rho_g)/\rho_m]^{1/2}, \ 0.85 < \alpha_{sl} < 1 \qquad (30)$$

$$\Rightarrow v_{gs} = 0.55K_g[(d_e + d_i)(\phi P - KP)/\phi P]^{1/2}$$

$$\Rightarrow v_{gs} = 0.55K_g[(d_e + d_i)(\phi - K)/\phi]^{1/2}, \quad 0.85 < \alpha_{sl} < 1 \qquad (31)$$

For slug flow in a vertical pipe (the chokeline), the void fraction is assumed constant and the relative slip velocity is calculated as

$$v_{gs} = 1.99[(\rho_m - \rho_g)d_i/\rho_m]^{1/2} \qquad (32)$$

$$=> v_{gs} = 1.99[(\phi P - KP)d_i/\phi P]^{1/2}$$

$$=> v_{gs} = 1.99[(\phi - K)d_i/\phi]^{1/2} \qquad (33)$$

Transition flow occurs if $\alpha_b < \alpha < \alpha_{sl}$. It is assumed to vary linearly with void fraction between bubble and slug flow regimes in order to avoid discontinuities during simulation.

3.4.4 Frictional pressure loss:

$$F = F(P, T, n, \alpha, s, v_m, v_s) \quad (34)$$

I. Single phase Flow

Frictional pressure losses for single phase flows are calculated from friction factor correlations used for non-Newtonian fluids, while two phase losses are calculated using correlations of mud/gas flows, or by modifying correlations used for Newtonian fluids. Also, localized pressure losses occur in choke and choke line, if used, and drill bit and at points of change of flow area. These are also modeled and included in the kick simulator [2].

For single phase flow, the frictional pressure loss gradient is given by [22],

$$F = \left(\frac{\Delta p}{\Delta s}\right)_f = \frac{\left(0.8066\ x\ 10^{-3}\right) f \rho_m v_m^2}{d_H} \quad (35)$$

The friction factor,f, is found from Blasius' correlation and modified for non-newtonian fluids using the power law model. f is found separately depending on whether flow is laminar or turbulent.

For laminar flow,

$$f = {}^{64}/_{Re}, \quad Re < Re_L = 3470 - 1370n \quad (36)$$

And for turbulent flow,

$$f = aRe^{-b}, \quad Re > Re_T = 4270 - 1370n \tag{37}$$

$$n = 3.32 \log\left[\frac{\sigma_{yp}+2\mu_p}{\sigma_{yp}+\mu_p}\right] \tag{38}$$

$$a = [\log(n) + 3.95]/12.5 \tag{39}$$

$$b = [1.75 - \log(n)]/7 \tag{40}$$

$$Re = [0.23{v_m}^{2-n}{d_H}^n\rho_m]/k(8)^{n-1} \tag{41}$$

Where,

$$k = \left[\frac{(\sigma_{yp}+2\mu_{p)k'}}{100(1022)^n}\right] \tag{42}$$

$k' = \left[\frac{2n+1}{2n}\right]^n$ for annulus, and (43)

$k' = \left[\frac{3n+1}{4n}\right]^n$ for drill string (44)

For transition region, a linear interpolation is obtained between laminar and turbulent region Reynolds numbers.

The hydraulic diameter is found thus:

For drillstring, $d_H = d$ (45)

For annulus, $d_H = d_e - d_i$ (46)

II. Multi-phase Flow [22, 23, 25]

The single phase friction pressure loss term is adjusted to account for the multi-phase nature of the fluid.

$$F = 2cf\rho_{mix}v_{mix}^2/d_H \quad (47)$$

Where coefficient,c, is a calibration factor that can be used to adjust the simulation model to real time measurements using a proper calibration technique [23]. Otherwise, the default value of c = 1, will be assumed in this model.

The friction pressure gradient is calculated using Beggs and Brill correlation to determine the friction factor, f, which is then plugged into the equation for friction pressure loss. This correlation is for steady state flow where gas and liquid fractions are known. To account for the transient nature of the model, the void fraction used is obtained directly from the model equations 1 to 3. The mixture density, velocity and friction factor are calculated as

$$\rho_{mix} = \rho_m(1-\alpha) + \rho_g\alpha \quad (48)$$

$$v_{mix} = v_m(1-\alpha) + v_g\alpha, \quad \text{for } K_g = 1 \quad (49)$$

$$f = f_n e^s \quad (50)$$

The no-slip friction factor, f_n, is dependent on the relative roughness of the pipe, ε/d_H, and the two-phase Reynold's number, Re. It can be read off the Moody chart, but is given by Beggs and Brill (1973) as [27]:

$$f_n = 1/[4\log\left(\frac{Re}{4.5223\log(Re)-3.8215}\right)]^2 \quad (51)$$

$$Re = \ 1488 d_H v_{mix} \rho_{mix} / \mu_{mix} \quad (52)$$

$$\mu_{mix} = \ \mu_m(1-\alpha) + \ \mu_g \alpha \ ; \quad (53)$$

$\mu_m = \ \mu_p \ =$ plastic viscosity of mud

$$s = \frac{\ln(x)}{\{-0.0523+3.182\ln(x)-0.8725[\ln(x)]^2+0.01853[\ln(x)]^4\}} \quad (54)$$

s is unbounded in the interval $1 < x < 1.2$, and for this interval

$$s = \ \ln(2.2x - 1.2) \quad (55)$$

$$x = \ \alpha_l / {y_l}^2 \quad (56)$$

$$\alpha_l = 1 - \ \alpha \quad (57)$$

$$y_l = y_o \psi \quad (58)$$

$$y_o = a{\alpha_l}^b / {N_{FR}}^c \quad (59)$$

$$N_{FR} = {v_{mix}}^2 / g d_H \quad (60)$$

$$\psi = \ 1 + C[\sin(1.8\theta) - 0.333\, sin^3(1.8\theta)]; \quad (61)$$

For vertical pipe, $\psi = 1$

The Beggs and Brill hold-up constants, a, b and c, are dependent on the kind of flow regime, thus:

Flow Regime	a	b	c
Segregated	0.98	0.4846	0.0868
Intermittent	0.845	0.5351	0.0173
Distributed	1.065	0.5824	0.0609

Table 2.1 Beggs and Brill Correlation Constants for Two-Phase Flows [26]

The flow regimes in this case are different in definition from the flow regimes used for the determination of the slip velocity, albeit it is still dependent on the void fraction (or liquid hold up as the case may be. To determine the flow regimes:

$$L_1 = 316\alpha_l^{0.302}\ ; \qquad L_2 = 0.0009252\alpha_l^{-2.4684}$$

$$L_3 = 0.1\alpha_l^{-1.4516}\ ; \qquad L_4 = 0.5\alpha_l^{-6.738} \tag{62}$$

Flow is segregated if $\alpha_l < 0.01$ and $N_{FR} < L_1$ OR $\alpha_l > 0.01$ and $N_{FR} > L_1$
This will be designated as Condition 1

Transition if $\alpha_l \geq 0.01$ and $L_2 < N_{FR} \leq L_1$
This will be designated as Condition 2

Intermittent if $0.01 \leq \alpha_l < 0.4$ and $L_3 < N_{FR} \leq L_1$

OR $\alpha_l \geq 0.4$ and $L_3 < N_{FR} \leq L_4$

This will be designated as Condition 3

Distributed if $\alpha_l < 0.4$ and $N_{FR} \geq L_1$ OR $\alpha_l \geq 0.01$ and $N_{FR} > L_4$

This will be designated as Condition 4. The logic for determining the flow regime and consequently, the Beggs and Brill constants to be applied, is depicted in Figure 3.6.

The transition flow values for a, b and c are found by linearly interpolating between segregated and intermittent flow values. [All correlations presented for friction factor calculation are in units of lb, ft, s and cp].

Let $Y = F$, the friction pressure gradient in (2) and (5) (63)

The slip velocity, v_{gs}, and friction pressure gradient, Y, are dependent on the dominant flow regime at any instant, which is in turn dependent on the values of the variables of interest at that instant. ϕ, the mud density coefficient, is also dependent on the pressure at any time and location. Hence, these coefficients and parameters are calculated in a separate sub-routine before they are fed into the conservation equations.

Substituting equations (17) and (63) into equations (1) and (2), we arrive at the two variables (P, v_m) for the two single phase conservation equations, thus:

Mass conservation of mud:

$$\frac{\partial}{\partial t}(A\phi P) + \frac{\partial}{\partial s}(A\phi P v_m) = 0 \quad (64)$$

Momentum Conservation:

$$\frac{\partial}{\partial t}(\phi P v_m) + \frac{\partial}{\partial s}(\phi P v_m^2) + \frac{\partial P}{\partial s} + Y - \phi P g cos\theta = 0 \quad (65)$$

Also, substituting equations (13), (17), (26) and (63) into equations (3), (4) and (5), we are left with three unknown variables (P, v_m and α) for the three conservation equations for two-phase flow. Thusly:

Mass conservation of Mud

$$\frac{\partial}{\partial t}(A(1-\alpha)\phi P) + \frac{\partial}{\partial s}(A(1-\alpha)\phi P v_m) = 0$$

$$=> A\phi \frac{\partial}{\partial t}\big(P(1-\alpha)\big) + A\phi \frac{\partial}{\partial s}\big(P v_m(1-\alpha)\big) = 0 \quad (66)$$

Mass conservation of Gas

$$\frac{\partial}{\partial t}(A\alpha K P) + \frac{\partial}{\partial s}\Big(A\alpha K P(v_m + \frac{v_{gs}}{(1-\alpha)})\Big) = 0$$

$$\Rightarrow AK \frac{\partial}{\partial t}(\alpha P) + AK \frac{\partial}{\partial s}\Big(\alpha P(v_m + \frac{v_{gs}}{(1-\alpha)})\Big) = 0 \quad (67)$$

Conservation of total momentum

$$\frac{\partial}{\partial t}\Bigg((1-\alpha)\phi P v_m + \alpha K P(v_m + \frac{v_{gs}}{(1-\alpha)})\Bigg) + \frac{\partial}{\partial s}\Bigg((1-\alpha)\phi P v_m^2 + \alpha K P(v_m + \frac{v_{gs}}{(1-\alpha)})^2\Bigg) + \frac{\partial P}{\partial s} + Y - \big((1-\alpha)\phi P + \alpha K P\big) g cos\theta = 0$$

$$=> \frac{\partial}{\partial t}\left(\phi P v_m(1-\alpha) + \alpha K P(v_m + \frac{v_{gs}}{(1-\alpha)})\right) + \frac{\partial}{\partial s}\left((1-\alpha)\phi P v_m^2 + \alpha K P(v_m + \frac{v_{gs}}{(1-\alpha)})^2\right) + \frac{\partial P}{\partial s} + Y - P(\phi - \alpha\phi + \alpha K) g cos\theta = 0 \quad (68)$$

A factor, $144g$ is added to the term $\frac{\partial P}{\partial s}$ so that it has the same units as all the other terms for rate of change of momentum $\frac{\partial}{\partial t}(\rho v)$, i.e. $\frac{lb}{ft^2}.\frac{1}{s^2}$, as will be shown later.

3.5 NUMERICAL DISCRETIZATION

A fully implicit, upwind, finite volume numerical approach is applied to the conservation equations and Newton iteration is used to solve the resulting discretized equations [29, 30]. A schematic of a single node and its boundaries and a succession of grid points is shown below. The location of parameters and variables are also indicated.

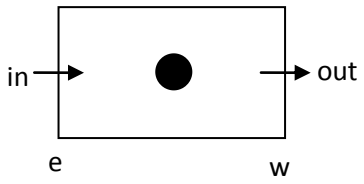

Fig. 3.7 - Single Node and its Boundaries

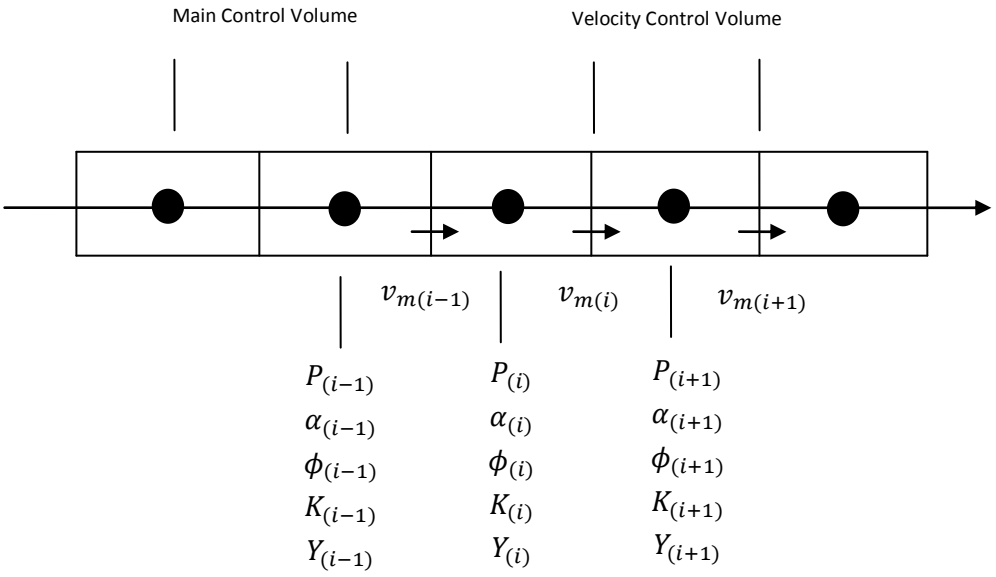

Fig. 3.8 - Finite Volume Schematic. The grid is staggered, with mud velocity defined at the boundaries of each grid element while pressure, void fraction and other parameters are defined at the node center.

The transient conservation equations are derived by integrating over the control volume from point x to point $x + \Delta x$ at time t to time $t + \Delta t$. We shall use i, $i + 1$, and $i - 1$ to denote current, next and previous positions respectively and n and $n + 1$ to denote previous and current time steps respectively.

3.5.1 Single Phase Discretization

3.5.1.1 Mass conservation of mud - Single Phase

From equation (64), we have

$$A\frac{\partial}{\partial t}(\phi P) + A\frac{\partial}{\partial s}(\phi P v_m) = 0$$

$$\int_{x}^{x+\Delta x} . \int_{t}^{t+\Delta t} \left[A\frac{\partial}{\partial t}(\phi P)\right] dt\, dx \;+\; \int_{t}^{t+\Delta t} . \int_{x}^{x+\Delta x} \left[A\frac{\partial}{\partial s}(\phi P v_m)\right] dx\, dt \;= 0$$

$$\Rightarrow A_i \frac{\Delta x}{\Delta t}\left[{\phi_i}^{n+1}{P_i}^{n+1} - {\phi_i}^{n}{P_i}^{n}\right] + \int_{t}^{t+\Delta t} \left[(A\phi P v_m)_e - (A\phi P v_m)_w\right] dt = 0$$

The points e and w refers to the east and west boundaries of any node point as shown in Figure 3.7, and the description with respect to i and $i+1$ varies depending on the solution method employed, as will be explained later.

Let f be a weighting factor from 0 to 1 that reflects the variation of the flux term with current and previous time.

$$\Rightarrow A_i \frac{\Delta x}{\Delta t}\left[{\phi_i}^{n+1}{P_i}^{n+1} - {\phi_i}^{n}{P_i}^{n}\right] + f\left[{(A\phi P v_m)_e}^{n+1} - {(A\phi P v_m)_w}^{n+1}\right]$$
$$+(1-f)\left[{(A\phi P v_m)_e}^{n} - {(A\phi P v_m)_w}^{n}\right] = 0$$

For the fully implicit scheme, $f = 1$

$$\Rightarrow A_i \frac{\Delta x}{\Delta t}\left[{\phi_i}^{n+1}{P_i}^{n+1} - {\phi_i}^{n}{P_i}^{n}\right] + {(A\phi P v_m)_e}^{n+1} - {(A\phi P v_m)_w}^{n+1} = 0$$

The upwind scheme assumes the value of the variables upstream of the flow direction. If flow is from left to right, the boundary or node points, e and w, become points i and $i-1$ respectively and if flow is from right to left points e and w become points $i+1$ and i respectively. The use of the $maximum$ function helps make the switch depending on whether the current velocity is greater or less than the previous velocity.

$$\Rightarrow A_i \frac{\Delta x}{\Delta t}\left[{\phi_i}^{n+1}{P_i}^{n+1} - {\phi_i}^{n}{P_i}^{n}\right] + \left[A_i P_i \phi_i \max\left(v_{m(i)}, 0\right)\right]^{n+1}$$
$$- \left[A_{i+1} P_{i+1} \phi_{i+1} \max\left(-v_{m(i)}, 0\right)\right]^{n+1} -$$
$$\left[A_{i-1} P_{i-1} \phi_{i-1} \max\left(v_{m(i-1)}, 0\right)\right]^{n+1} + \left[A_i P_i \phi_i \max\left(-v_{m(i-1)}, 0\right)\right]^{n+1} = 0$$

Removing the superscript $n+1$, we denote current time without superscript and previous time with superscript n.

$$\Rightarrow A_i \frac{\Delta x}{\Delta t}\left[\phi_i P_i - {\phi_i}^{n}{P_i}^{n}\right]$$
$$+ A_i P_i \phi_i \max\left(v_{m(i)}, 0\right) - A_{i+1} P_{i+1} \phi_{i+1} \max\left(-v_{m(i)}, 0\right)$$
$$+ A_{i-1} P_{i-1} \phi_{i-1} \max\left(v_{m(i-1)}, 0\right) + A_i P_i \phi_i \max\left(-v_{m(i-1)}, 0\right) = 0 \qquad (69)$$

3.5.1.2 Momentum Conservation - Single Phase

From equation (65), we have

$$\frac{\partial}{\partial t}(\phi P v_m) + \frac{\partial}{\partial s}(\phi P v_m^2) + 144g\frac{\partial P}{\partial s} + Y - \phi P g cos\theta = 0$$

(The factor, 144, converts psi to psft. Gravity, g, makes units of dP/ds same as all other terms in the equation.)

$$\int_x^{x+\Delta x} . \int_t^{t+\Delta t} \left[\frac{\partial}{\partial t}(\phi P v_m)\right] dt$$
$$+ \int_t^{t+\Delta t} . \int_x^{x+\Delta x} \left[\frac{\partial}{\partial s}(\phi P v_m^2)\right] dx\, dt$$
$$+ \int_t^{t+\Delta t} . \int_x^{x+\Delta x} 144g\frac{\partial P}{\partial s}\, dt\, dx + \int_t^{t+\Delta t} . \int_x^{x+\Delta x} [Y - \phi P g cos\theta] dt\, dx = 0$$

$$\Delta x[\phi_i{}^{n+1} P_i{}^{n+1} v_{m(i)}{}^{n+1}] - \Delta x[\phi_i{}^{n} P_i{}^{n} v_{m(i)}{}^{n}] + \int_t^{t+\Delta t} .[(\phi P v_m^2)_e - (\phi P v_m^2)_w]dt$$
$$+ \int_t^{t+\Delta t} .144g(P_e - P_w)\, dt + \int_t^{t+\Delta t} .\Delta x(Y - \phi P g cos\theta)dt = 0$$

Using the weighting factor, f, that reflects the variation of the flux term with current and previous time, and assigning $f = 1$ for the implicit scheme, we get

$$\frac{\Delta x}{\Delta t}[\phi_i{}^{n+1} P_i{}^{n+1} v_{m(i)}{}^{n+1}] - \Delta x[\phi_i{}^{n} P_i{}^{n} v_{m(i)}{}^{n}] + (\phi P v_m^2)_e{}^{n+1} - (\phi P v_m^2)_w{}^{n+1}$$
$$+ 144g(P_e{}^{n+1} - P_w{}^{n+1}) + \Delta x[Y - \phi P g cos\theta]^{n+1} = 0$$

Using the same superscript notation we used earlier for current and previous time, we get

$$\frac{\Delta x}{\Delta t}[\phi_i P_i v_{m(i)}] - \Delta x[\phi_i{}^{n} P_i{}^{n} v_{m(i)}{}^{n}] + (\phi P v_m^2)_e - (\phi P v_m^2)_w + 144g(P_e - P_w)$$
$$+ \Delta x[Y - \phi P g cos\theta] = 0$$

The velocity in the flux term is squared. This presents a problem in determining the direction of flow, since even if direction is negative, this determination disappears when the term is squared. A different approach is used. It is to evaluate the flux terms at the node point and the storage term at the grid boundaries. The body forces are evaluated at the boundaries as should be. This is done by taking a simple average of the parameter at the said point [29]. Hence the momentum equation becomes

$$\frac{\Delta x}{\Delta t}[v_{m(i)}\left(\frac{\phi_i+\phi_{i+1}}{2}\right)\left(\frac{P_i+P_{i+1}}{2}\right)]$$
$$-\Delta x[{v_{m(i)}}^n\left(\frac{\phi_i+\phi_{i+1}}{2}\right)^n\left(\frac{P_i+P_{i+1}}{2}\right)^n]+\left(\phi_{i+1}P_{i+1}\left(\frac{v_{m(i)}+v_{m(i+1)}}{2}\right)^2\right)$$
$$-\left(\phi_iP_i\left(\frac{v_{m(i)}+v_{m(i-1)}}{2}\right)^2\right)+144g(P_{i+1}-P_i)$$
$$+\Delta x\left[(\frac{Y_i+Y_{i+1}}{2})-(\frac{P_i+P_{i+1}}{2})\left(\frac{\phi_i+\phi_{i+1}}{2}\right)gcos\theta\right]=0 \quad (70)$$

3.5.2 Two Phase Discretization

3.5.2.1 Mass Conservation of Mud - Two Phase

From equation (66), we have

$$A\frac{\partial}{\partial t}\left(\phi P(1-\alpha)\right)+A\frac{\partial}{\partial s}\left(\phi P v_m(1-\alpha)\right)=0$$

$$\int_x^{x+\Delta x}.\int_t^{t+\Delta t}\left[A\frac{\partial}{\partial t}\left(\phi P(1-\alpha)\right)\right]dt\,dx+\int_t^{t+\Delta t}.\int_x^{x+\Delta x}\left[A\frac{\partial}{\partial s}\left(\phi P v_m(1-\alpha)\right)\right]dx\,dt=0$$

$$\Rightarrow A_i\frac{\Delta x}{\Delta t}\left[{\phi_i}^{n+1}{P_i}^{n+1}(1-{\alpha_i}^{n+1})-{\phi_i}^n{P_i}^n(1-{\alpha_i}^n)\right]$$

$$+\int_t^{t+\Delta t}[\left(A\phi P v_m(1-\alpha)\right)_e-\left(A\phi P v_m(1-\alpha)\right)_w]\,dt=0$$

The points e and w refer to the east and west boundaries of any node point and the description with respect to i and $i+1$ varies depending on the solution method employed, as will be explained later.

Let f be a weighting factor from 0 to 1 that reflects the variation of the flux term with current and previous time.

$$\Rightarrow A_i \frac{\Delta x}{\Delta t}\left[{\phi_i}^{n+1}{P_i}^{n+1}(1-{\alpha_i}^{n+1}) - {\phi_i}^{n}{P_i}^{n}(1-{\alpha_i}^{n})\right]$$
$$+ f\left[\left(A\phi P v_m(1-\alpha)\right)_e^{\,n+1} - \left(A\phi P v_m(1-\alpha)\right)_w^{\,n+1}\right]$$
$$+(1-f)\left[\left(A\phi P v_m(1-\alpha)\right)_e^{\,n} - \left(A\phi P v_m(1-\alpha)\right)_w^{\,n}\right] = 0$$

For the fully implicit scheme, $f = 1$

$$\Rightarrow A_i \frac{\Delta x}{\Delta t}\left[{\phi_i}^{n+1}{P_i}^{n+1}(1-{\alpha_i}^{n+1}) - {\phi_i}^{n}{P_i}^{n}(1-{\alpha_i}^{n})\right]$$
$$+ \left(A\phi P v_m(1-\alpha)\right)_e^{\,n+1} - \left(A\phi P v_m(1-\alpha)\right)_w^{\,n+1} = 0$$

The upwind scheme assumes the value of the variables upstream of the flow direction. If flow is from left to right, the boundary or node points, e and w, become points i and $i-1$ respectively and if flow is from right to left points e and w become points $i+1$ and i respectively. The use of the $maximum$ function helps make the switch depending on whether the current velocity is greater or less than the previous velocity.

$$\Rightarrow A_i \frac{\Delta x}{\Delta t}\left[{\phi_i}^{n+1}{P_i}^{n+1}(1-{\alpha_i}^{n+1}) - {\phi_i}^{n}{P_i}^{n}(1-{\alpha_i}^{n})\right] +$$
$$[A_i P_i \phi_i (1-\alpha_i)\max(v_{m(i)}, 0)]^{n+1} - [A_{i+1} P_{i+1} \phi_{i+1}(1-\alpha_{i+1})\max(-v_{m(i)}, 0)]^{n+1} -$$
$$[A_{i-1} P_{i-1} \phi_{i-1}(1-\alpha_{i-1})\max(v_{m(i-1)}, 0)]^{n+1}$$
$$+ [A_i P_i \phi_i (1-\alpha_i)\max(-v_{m(i-1)}, 0)]^{n+1} = 0$$

Removing the superscript $n+1$, we denote current time without superscript and previous time with superscript n.

$$\Rightarrow A_i \frac{\Delta x}{\Delta t}\left[\phi_i P_i(1-\alpha_i) - {\phi_i}^n {P_i}^n(1-{\alpha_i}^n)\right]$$
$$+ A_i P_i \phi_i (1-\alpha_i)\max\left(v_{m(i)}, 0\right) - A_{i+1} P_{i+1} \phi_{i+1}(1-\alpha_{i+1})\max\left(-v_{m(i)}, 0\right)$$
$$+ A_{i-1} P_{i-1} \phi_{i-1}(1-\alpha_{i-1})\max\left(v_{m(i-1)}, 0\right) + A_i P_i \phi_i (1-\alpha_i)\max\left(-v_{m(i-1)}, 0\right) = 0 \quad (71)$$

3.5.2.2 Mass Conservation of Gas - Two Phase

From equation (67), we have

$$A\frac{\partial}{\partial t}(\alpha K P) + A\frac{\partial}{\partial s}\left(\alpha K P\left(v_m + \frac{v_{gs}}{(1-\alpha)}\right)\right) = 0$$

$$\int_x^{x+\Delta x} \cdot \int_t^{t+\Delta t} \left[A\frac{\partial}{\partial t}(\alpha K P)\right] dt\, dx$$
$$+ \int_t^{t+\Delta t} \cdot \int_x^{x+\Delta x} \left[A\frac{\partial}{\partial s}\left(\alpha K P\left(v_m + \frac{v_{gs}}{(1-\alpha)}\right)\right)\right] dx\, dt \quad = 0$$

$$\Rightarrow A_i \frac{\Delta x}{\Delta t}\left[{\alpha_i}^{n+1} {K_i}^{n+1} {P_i}^{n+1} - {\alpha_i}^n {K_i}^n {P_i}^n\right]$$

$$+ \int_t^{t+\Delta t}\left[\left(A\alpha K P\left(v_m + \frac{v_{gs}}{(1-\alpha)}\right)\right)_e - \left(A\alpha K P\left(v_m + \frac{v_{gs}}{(1-\alpha)}\right)\right)_w\right] dt = 0$$

The points *e* and *w* refers to the east and west boundaries of any node point and the description with respect to i and $i+1$ varies depending on the solution method employed, as will be explained later.

Let f be a weighting factor from 0 to 1 that reflects the variation of the flux term with current and previous time.

$$\Rightarrow A_i \frac{\Delta x}{\Delta t}\left[{\alpha_i}^{n+1}{K_i}^{n+1}{P_i}^{n+1} - {\alpha_i}^{n}{K_i}^{n}{P_i}^{n}\right]$$
$$+ f\left[\left(A\alpha KP(v_m + \frac{v_{gs}}{(1-\alpha)})\right)_e^{n+1} - \left(A\alpha KP(v_m + \frac{v_{gs}}{(1-\alpha)})\right)_w^{n+1}\right]$$
$$+(1-f)\left[\left(A\alpha KP(v_m + \frac{v_{gs}}{(1-\alpha)})\right)_e^{n} - \left(A\alpha KP(v_m + \frac{v_{gs}}{(1-\alpha)})\right)_w^{n}\right]$$
$$= 0$$

For the fully implicit scheme, $f = 1$

$$\Rightarrow A_i \frac{\Delta x}{\Delta t}\left[{\alpha_i}^{n+1}{K_i}^{n+1}{P_i}^{n+1} - {\alpha_i}^{n}{K_i}^{n}{P_i}^{n}\right]$$
$$+ \left(A\alpha KP(v_m + \frac{v_{gs}}{(1-\alpha)})\right)_e^{n+1} - \left(A\alpha KP(v_m + \frac{v_{gs}}{(1-\alpha)})\right)_w^{n+1}$$

Using the same definition for the upwind scheme as before,

$$\Rightarrow A_i \frac{\Delta x}{\Delta t}\left[{\alpha_i}^{n+1}{K_i}^{n+1}{P_i}^{n+1} - {\alpha_i}^{n}{K_i}^{n}{P_i}^{n}\right] + [A_i\alpha_i K_i P_i(\max((v_{m(i)} + \frac{v_{gs(i)}}{(1-\alpha_i)}),0)]^{n+1}$$
$$- [A_{i+1}\alpha_{i+1}K_{i+1}P_{i+1}\max(-(v_{m(i)} + \frac{v_{gs(i+1)}}{(1-\alpha_{i+1})}),0)]^{n+1}$$
$$-[A_{i-1}\alpha_{i-1}K_{i-1}P_{i-1}\max((v_{m(i-1)} + \frac{v_{gs(i-1)}}{(1-\alpha_{i-1})}),0)]^{n+1}$$
$$+ [A_i\alpha_i K_i P_i\max(-(v_{m(i-1)} + \frac{v_{gs(i)}}{(1-\alpha_i)}),0)]^{n+1} = 0$$

Removing the superscript $n+1$, we denote current time without superscript and previous time with superscript n.

$$\Rightarrow A_i \frac{\Delta x}{\Delta t}\left[\alpha_i K_i P_i - {\alpha_i}^n {K_i}^n {P_i}^n\right]$$

$$+ A_i\alpha_i K_i P_i \max\left((v_{m(i)} + \frac{v_{gs(i)}}{(1-\alpha_i)}),0\right) - A_{i+1}\alpha_{i+1}K_{i+1}P_{i+1}\max\left(-(v_{m(i)} + \frac{v_{gs(i+1)}}{(1-\alpha_{i+1})}),0\right)$$

$$+A_{i-1}\alpha_{i-1}K_{i-1}P_{i-1}\max\left((v_{m(i-1)} + \frac{v_{gs(i-1)}}{(1-\alpha_{i-1})}),0\right) + A_i\alpha_i K_i P_i \max\left(-(v_{m(i-1)} + \frac{v_{gs(i)}}{(1-\alpha_i)}),0\right) = 0 \quad (72)$$

3.5.2.3 Momentum Conservation - Two Phase

From equation (68), we have

$$\frac{\partial}{\partial t}\left(\phi P v_m(1-\alpha) + \alpha K P(v_m + \frac{v_{gs}}{(1-\alpha)})\right) + \frac{\partial}{\partial s}\left((1-\alpha)\phi P v_m^2 + \alpha K P(v_m + \frac{v_{gs}}{(1-\alpha)})^2\right) + 144g\frac{\partial P}{\partial s} + Y - P(\phi - \alpha\phi + \alpha K)g\cos\theta = 0$$

(The factor, 144, converts psi to psft and g makes units of dP/ds same as all other terms in the equation.)

$$\int_x^{x+\Delta x}\int_t^{t+\Delta t}\left[\frac{\partial}{\partial t}\left(\phi P v_m(1-\alpha) + \alpha K P(v_m + \frac{v_{gs}}{(1-\alpha)})\right)\right]dt\,dx$$

$$+ \int_t^{t+\Delta t}\int_x^{x+\Delta x}\left[\frac{\partial}{\partial s}\left((1-\alpha)\phi P v_m^2 + \alpha K P(v_m + \frac{v_{gs}}{(1-\alpha)})^2\right)\right]dx\,dt$$

$$+ \int_t^{t+\Delta t}\int_x^{x+\Delta x} 144g\frac{\partial P}{\partial s}\,dt\,dx$$

$$+ \int_t^{t+\Delta t}\int_x^{x+\Delta x}[Y - P(\phi - \alpha\phi + \alpha K)g\cos\theta]dt\,dx = 0$$

$$\Delta x[{\phi_i}^{n+1}{P_i}^{n+1}{v_{m(i)}}^{n+1}(1-{\alpha_i}^{n+1})+\ {\alpha_i}^{n+1}{K_i}^{n+1}{P_i}^{n+1}({v_{m(i)}}^{n+1}+\frac{{v_{gs(i)}}^{n+1}}{(1-{\alpha_i}^{n+1})})]$$

$$-\ \Delta x[{\phi_i}^{n}{P_i}^{n}{v_{m(i)}}^{n}(1-{\alpha_i}^{n})+\ {\alpha_i}^{n}{K_i}^{n}{P_i}^{n}({v_{m(i)}}^{n}+\frac{{v_{gs(i)}}^{n}}{(1-{\alpha_i}^{n})})]$$

$$+\int_t^{t+\Delta t}.\left[\left((1-\alpha)\phi P v_m^2+\ \alpha KP(v_m+\frac{v_{gs}}{(1-\alpha)})^2\right)_e\right.$$

$$\left.-\left((1-\alpha)\phi P v_m^2+\ \alpha KP(v_m+\frac{v_{gs}}{(1-\alpha)})^2\right)_w\right]dt+\int_t^{t+\Delta t}.144g(P_e$$

$$-\ P_w)\ dt+\int_t^{t+\Delta t}.\Delta x(Y-\ P(\phi-\alpha\phi+\alpha K)gcos\theta)dt=0$$

Using the weighting factor, f, that reflects the variation of the flux term with current and previous time, and assigning $f=1$ for the implicit scheme, we get

$$\frac{\Delta x}{\Delta t}[{\phi_i}^{n+1}{P_i}^{n+1}{v_{m(i)}}^{n+1}(1-{\alpha_i}^{n+1})+\ {\alpha_i}^{n+1}{K_i}^{n+1}{P_i}^{n+1}({v_{m(i)}}^{n+1}+\frac{{v_{gs(i)}}^{n+1}}{(1-{\alpha_i}^{n+1})})]$$

$$-\ \Delta x[{\phi_i}^{n}{P_i}^{n}{v_{m(i)}}^{n}(1-{\alpha_i}^{n})+\ {\alpha_i}^{n}{K_i}^{n}{P_i}^{n}({v_{m(i)}}^{n}+\frac{{v_{gs(i)}}^{n}}{(1-{\alpha_i}^{n})})]$$

$$+\left((1-\alpha)\phi P v_m^2+\ \alpha KP(v_m+\frac{v_{gs}}{(1-\alpha)})^2\right)_e^{n+1}$$

$$-\left((1-\alpha)\phi P v_m^2+\ \alpha KP(v_m+\frac{v_{gs}}{(1-\alpha)})^2\right)_w^{n+1}+\ 144g({P_e}^{n+1}$$

$$-\ {P_w}^{n+1})+\ \Delta x[Y-\ P(\phi-\alpha\phi+\alpha K)gcos\theta]^{n+1}=0$$

Using the same superscript notation we used earlier for current and previous time, we get

$$\frac{\Delta x}{\Delta t}[\phi_i P_i v_{m(i)}(1-\alpha_i) + \alpha_i K_i P_i(v_{m(i)} + \frac{v_{gs(i)}}{(1-\alpha_i)})] - \Delta x[{\phi_i}^n {P_i}^n {v_{m(i)}}^n(1-{\alpha_i}^n) + {\alpha_i}^n {K_i}^n {P_i}^n({v_{m(i)}}^n + \frac{{v_{gs(i)}}^n}{(1-{\alpha_i}^n)})] + \left((1-\alpha)\phi P v_m^2 + \alpha K P(v_m + \frac{v_{gs}}{(1-\alpha)})^2\right)_e - \left((1-\alpha)\phi P v_m^2 + \alpha K P(v_m + \frac{v_{gs}}{(1-\alpha)})^2\right)_w + 144g(P_e - P_w) + \Delta x[Y - P(\phi - \alpha\phi + \alpha K)g\cos\theta] = 0$$

The velocity in the flux term is squared. This presents a problem in determining the direction of flow, since even if direction is negative, this determination disappears when the term is squared. A different approach is used. It is to evaluate the flux terms at the node point and the storage term at the grid boundaries. The body forces are evaluated at the boundaries as should be. This is done by taking a simple average of the parameter at the said point [29]. Hence the momentum equation becomes

$$\frac{\Delta x}{\Delta t}[v_{m(i)}(\frac{\phi_i+\phi_{i+1}}{2})(\frac{P_i+P_{i+1}}{2})\left(1-\left(\frac{\alpha_i+\alpha_{i+1}}{2}\right)\right) + (\frac{\alpha_i+\alpha_{i+1}}{2})(\frac{K_i+K_{i+1}}{2})(\frac{P_i+P_{i+1}}{2})(v_{m(i)} + \frac{v_{gs(i)}+v_{gs(i+1)}}{(2-\alpha_i-\alpha_{i+1})})] - \Delta x[{v_{m(i)}}^n\left(\frac{\phi_i+\phi_{i+1}}{2}\right)^n\left(\frac{P_i+P_{i+1}}{2}\right)^n\left(1-\left(\frac{\alpha_i+\alpha_{i+1}}{2}\right)^n\right) + \left(\frac{\alpha_i+\alpha_{i+1}}{2}\right)^n\left(\frac{K_i+K_{i+1}}{2}\right)^n\left(\frac{P_i+P_{i+1}}{2}\right)^n({v_{m(i)}}^n + \left(\frac{v_{gs(i)}+v_{gs(i+1)}}{(2-\alpha_i-\alpha_{i+1})}\right)^n)] + \left((1-\alpha_{i+1})\phi_{i+1}P_{i+1}\left(\frac{v_{m(i)}+v_{m(i+1)}}{2}\right)^2 + \alpha_{i+1}K_{i+1}P_{i+1}\left(\left(\frac{v_{m(i)}+v_{m(i+1)}}{2}\right) + \frac{v_{gs(i+1)}}{(1-\alpha_{i+1})}\right)^2\right) - \left((1-\alpha_i)\phi_i P_i\left(\frac{v_{m(i)}+v_{m(i-1)}}{2}\right)^2 +$$

$$\alpha_i K_i P_i \left(\left(\frac{v_{m(i)} + v_{m(i-1)}}{2} \right) + \frac{v_{gs(i)}}{(1-\alpha_i)} \right)^2 + 144g(P_{i+1} - P_i) + \Delta x \left[\left(\frac{Y_i + Y_{i+1}}{2} \right) - \left(\frac{P_i + P_{i+1}}{2} \right) \left(\left(\frac{\phi_i + \phi_{i+1}}{2} \right) \left(1 - \left(\frac{\alpha_i + \alpha_{i+1}}{2} \right) \right) + \left(\frac{\alpha_i + \alpha_{i+1}}{2} \right) \left(\frac{K_i + K_{i+1}}{2} \right) \right) g cos\theta \right] = 0 \qquad (72)$$

3.6 BOUNDARY CONDITIONS

For the solution of the transient equations described above, appropriate boundary and initial conditions must be defined. The figure below helps in the visualization of what parameter and variable values are needed at the initial time and at the boundaries to find the variables of interest at any point in time and space.

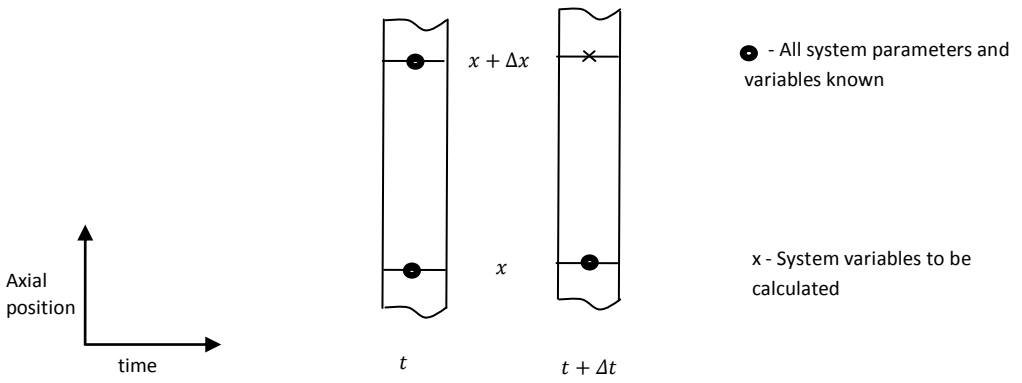

Figure 3.9 – Known and unknown parameter and variables with respect to time and position

Our interest is only in kick detection and this closely models an uncontrolled blowout. The well control process that occurs after kick is detected is not of interest at this point. Hence the boundary conditions are the constant pump inflow rate which specifies the mud velocity, v_m, at the bottomhole, and the annular surface pressure

which is equivalent to atmospheric pressure [22, 31]. The initial conditions at the start of kick are the single phase steady state mud velocity and pressure. A small amount of gas may be assumed to be present in the mud at this time.

$$v_{m(t,0)} = v_{inlet}$$
$$P_{(t,n)} = P_{atm}$$
$$P_{(0,x)} = P_{steady\ state}$$
$$v_{m(0,x)} = v_{m(steady\ state)}$$
$$\alpha_{(0,x)} = constant \quad (73)$$

The boundary condition for the void fraction, $\alpha_{(t,0)}$, is specified at the bottomhole at the start of kick by the rate of gas influx from the reservoir. This sets up a boundary condition at the inlet similar to the second kind or Neumann boundary condition, but with a time-dependent, non-constant flow rate.

3.6.1 Gas influx rate:

$$q = q(P, s, t, k, \varphi) \quad (74)$$

Reservoir-well interactions could lead to gas influx from the reservoir in an underbalance situation, or lost circulation when fracture pressure is exceeded. The rate of gas influx is driven by pore and bottomhole pressure imbalance as well as reservoir, fluid and geometric properties.

A transient gas-flow equation for an infinite well with constant reservoir pressure is used to specify the flow. This is given in field units by [32]

$$q_g = \frac{1000kh(P_p^2 - P_{bh}^2)}{(50300)(86400)p_D \mu_g P_{bh}} \quad (75)$$

where,

$$h = (ROP)t \tag{76}$$

$$p_D = 0.5[\ln(t_D) + 0.81) \tag{77}$$

$$t_D = \frac{(7.3167)10^{-8}kt}{\varphi \mu_g c_t r_w^2} \tag{78}$$

Model assumptions are that there is no pressure response from the reservoir during the transient period and also that the reservoir is radial and symmetric around the well.

It is known from Darcy's law that the gas influx rate is mainly driven by the fluid potential (pressure difference) and the permeability of the reservoir [33, 32]. An investigation into the degree of sensitivity of gas influx rate to reservoir properties revealed that reservoir porosity, on the other hand, has a lot less effect on the influx rate into the wellbore.

One of the indications of gas kicks is increased rate of penetration, and this can be traced to an increase in the pressure differential. Normally, while drilling, the rate of penetration experiences a slight and gradual decrease due to wear of the drilling bit until the drilling bit is changed. This cycle resumes after some time. A gradual and consistent increase in the rate of penetration could be an indication that a more porous shale region has been encountered, while a rapid increase in rate of penetration could be an indication that a abnormally pressured formation has been encountered. The latter could quickly result in an underbalance and gas kick would begin.

Once the influx starts however, the pressure differential and permeability play a greater role in determining the volume flow rate of fluid into the annulus of the wellbore. The time period before the well is brought under control, obviously, also affects the volume of influx. This is illustrated in Figures 3.10 through 3.12.

As can be observed in Figure 3.10, a 66.67% increase in pressure differential from pore pressure = bottomhole pressure + 180psi to pore pressure = bottomhole pressure + 300psi results in slightly over an exact increase (67.4%) in gas influx from 0.092 cu-ft/s to 0.153 cu-ft/s within the space of 30 seconds while keeping all other parameters constant. The same 66.67% increase in permeability from 300md to 500md for the same time period also results in almost an exact increase (53.4%) in gas influx rate from 0.153 cu-ft/s to 0.235 cu-ft/s (Figure 3.11). However, when the porosity of the reservoir was increased by the same 66.67% from 0.3 to 0.5, only a 9.4% increase in gas influx rate was observed for the same time period. This can be observed in Figure 3.12. While this demonstrates that pressure differential and permeability are the more important drivers of the rate of gas influx into a wellbore, it also serves as a guide on what to expect in trying to match simulation results to real-life data. Reservoir properties used must be a match in order to better analyze the accuracy or otherwise of simulated results.

By definition,

$$q_g = \frac{dV_g}{dt} = Av_g \tag{79}$$

The void fraction, α, at the bottomhole is thus defined as

$$\alpha_{(t,0)} = \frac{V_g}{V_g + V_m} = \frac{v_g}{v_g + v_m} = \frac{Av_g}{A(v_g + v_m)} = \frac{q_g}{q_g + q_m} \tag{80}$$

$$q_m = Av_m \tag{81}$$

where,

q_m is the mud flow rate at the well-reservoir interface, A is the area of the annulus at the bottomhole of the well, V_g is the volume of gas influx, and v_m is the mud velocity at

the bottomhole of the well. v_m at this point, is the fixed boundary condition specified by the pump inflow rate as described earlier.

3.7 SOLUTION PROCEDURE

Assigning the mud mass conservation equation as $F1$, the gas mass conservation equation as $F2$, and the momentum conservation equation as $F3$, a non-linear system of equations is obtained. The Newton iteration solution procedure is used to solve the equations [29] with the variables being annulus pressure, P, mud velocity, v_m, and gas void fraction, α. A Jacobian matrix, J, and a residual vector, R, are constructed as defined below.

$$J = \begin{bmatrix} \frac{\partial F_1}{\partial P} & \frac{\partial F_1}{\partial \alpha} & \frac{\partial F_1}{\partial v_m} \\ \frac{\partial F_2}{\partial P} & \frac{\partial F_2}{\partial \alpha} & \frac{\partial F_2}{\partial v_m} \\ \frac{\partial F_3}{\partial P} & \frac{\partial F_3}{\partial \alpha} & \frac{\partial F_3}{\partial v_m} \end{bmatrix} \tag{82}$$

Where, for example

$$\frac{\partial F_1}{\partial P} = \begin{bmatrix} \frac{\partial F_1}{\partial P_1} & \frac{\partial F_1}{\partial P_{i+1}} & 0 \\ \frac{\partial F_1}{\partial P_{i-1}} & \frac{\partial F_1}{\partial P_i} & \frac{\partial F_1}{\partial P_{i+1}} \\ 0 & \frac{\partial F_1}{\partial P_{n-1}} & \frac{\partial F_1}{\partial P_n} \end{bmatrix} \tag{83}$$

The matrix of functions, R, is given by

$$R = \begin{bmatrix} F_{1(1)} \\ F_{1(i)} \\ \vdots \\ F_{1(n)} \\ F_{2(1)} \\ F_{2(i)} \\ \vdots \\ F_{2(n)} \\ F_{3(1)} \\ F_{3(i)} \\ \vdots \\ F_{3(n)} \end{bmatrix} \tag{84}$$

Finally, the change in vector of variables is defined as

$$Z = \begin{bmatrix} \Delta P_1 \\ \Delta P_i \\ \vdots \\ \Delta P_n \\ \Delta \alpha_1 \\ \Delta \alpha_i \\ \vdots \\ \Delta \alpha_n \\ \Delta v_{m(1)} \\ \Delta v_{m(i)} \\ \vdots \\ \Delta v_{m(n)} \end{bmatrix} \tag{85}$$

Then by Newton's method,

$$Z = -R/J \tag{86}$$

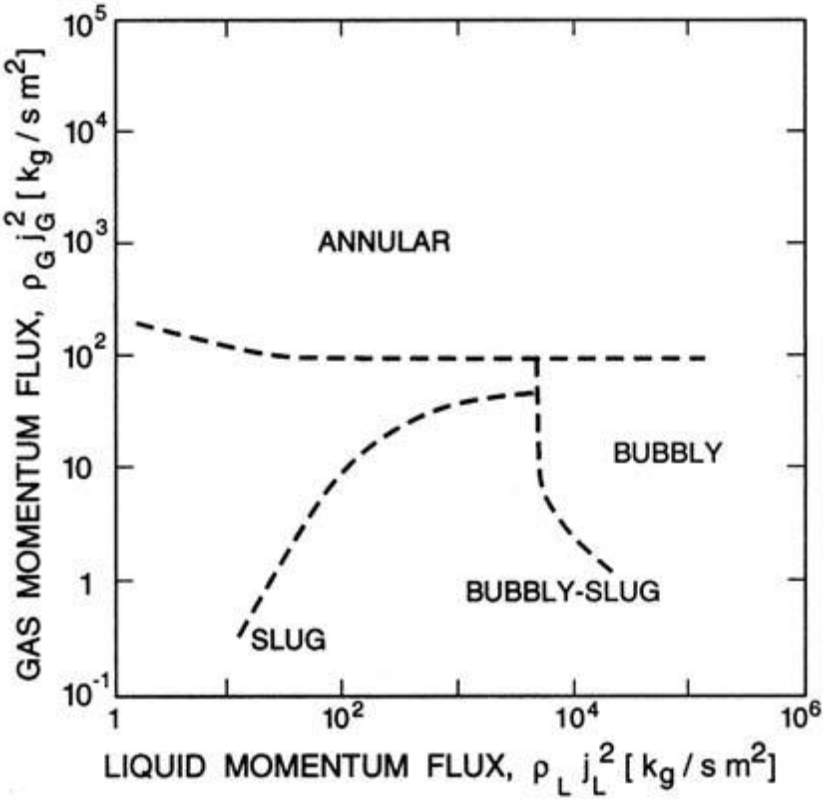

Figure 3.1 Vertical flow regime map of Hewitt and Roberts (1969) for flow in a 3.2cm diameter tube, validated for both air/water flow at atmospheric pressure and steam/water flow at high pressure [34]

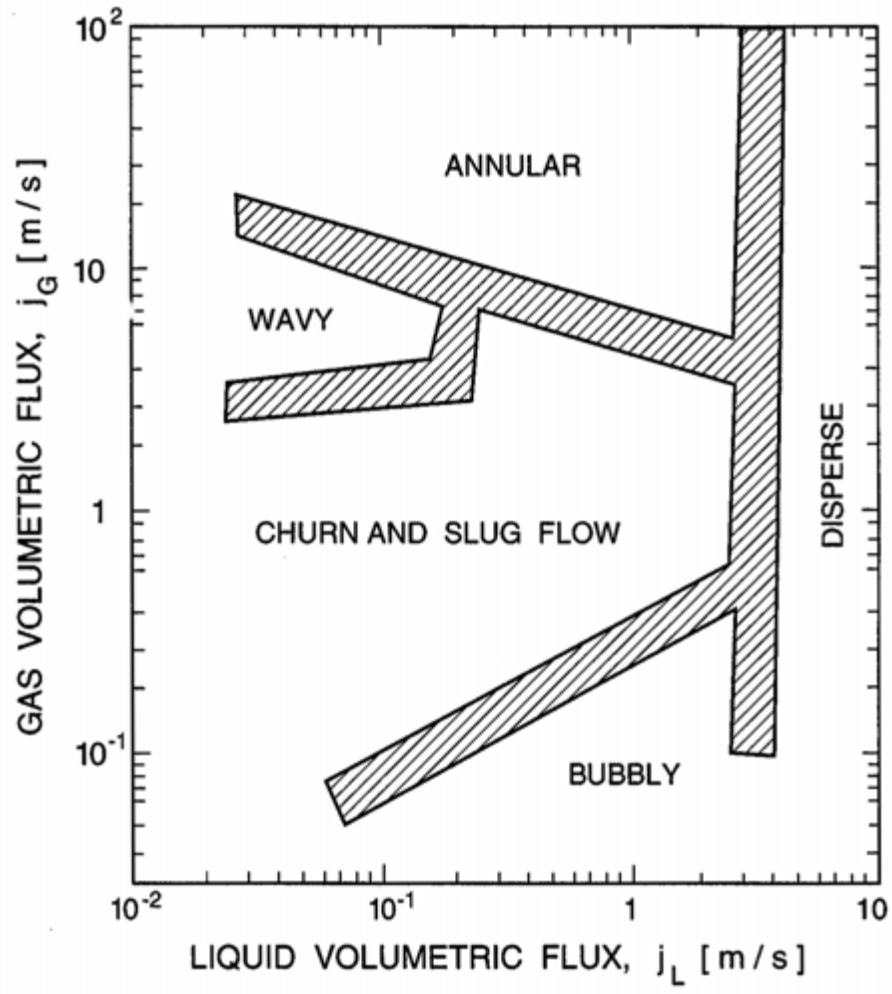

Figure 3.2 Flow regime map for the flow of air/water mixture in a vertical 2.5cm diameter pipe showing the experimentally observed transition regions hatched [34].

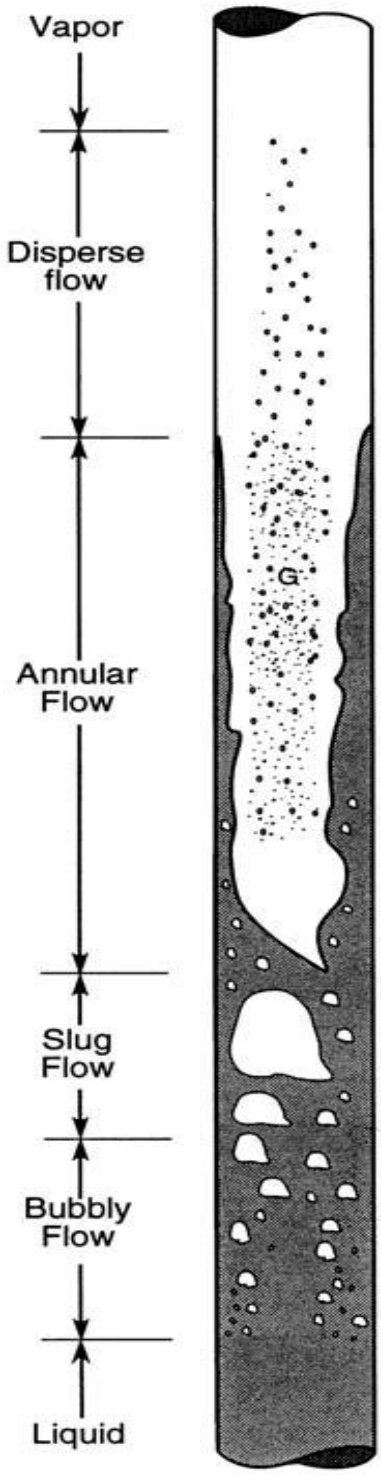

Figure 3.3 Vertical pipe flow regimes. Source [34]

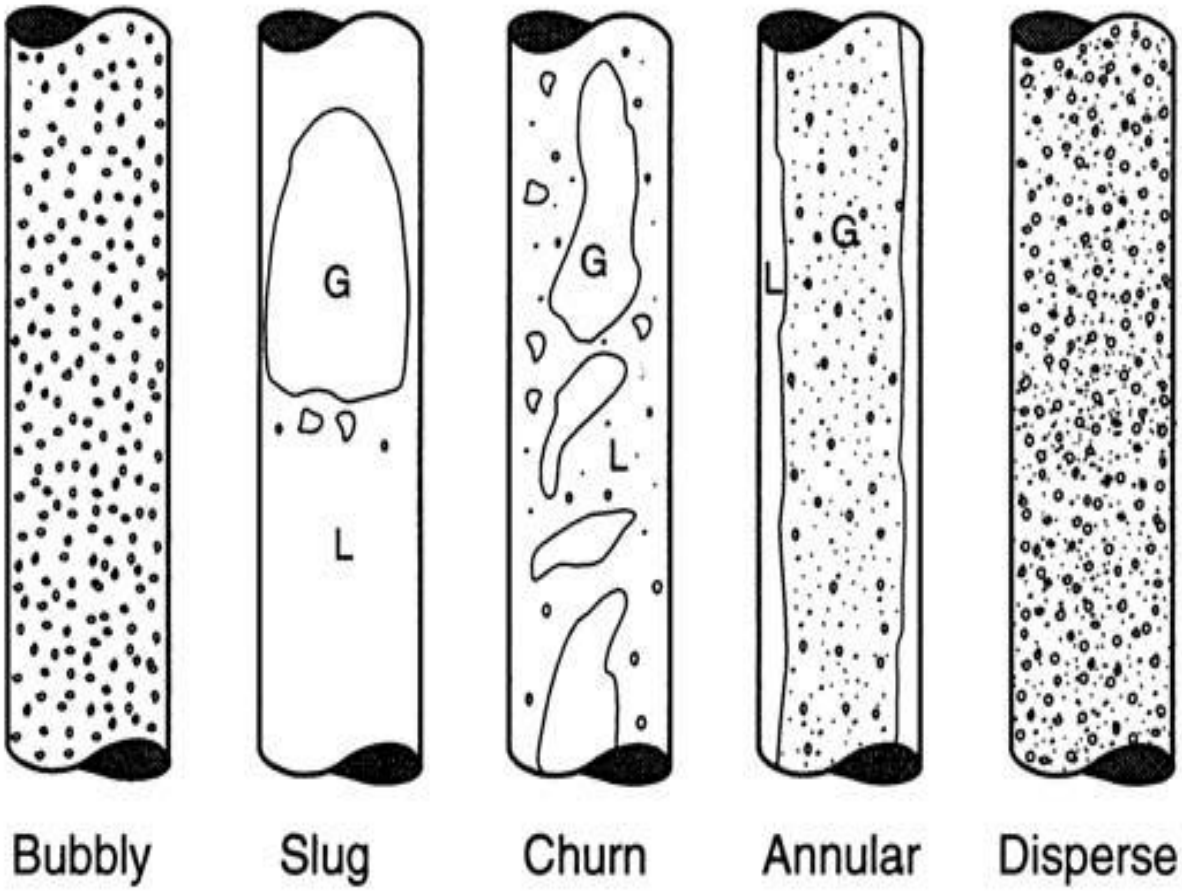

Figure 3.4 Vertical pipe flow regimes (detailed). Source [34]

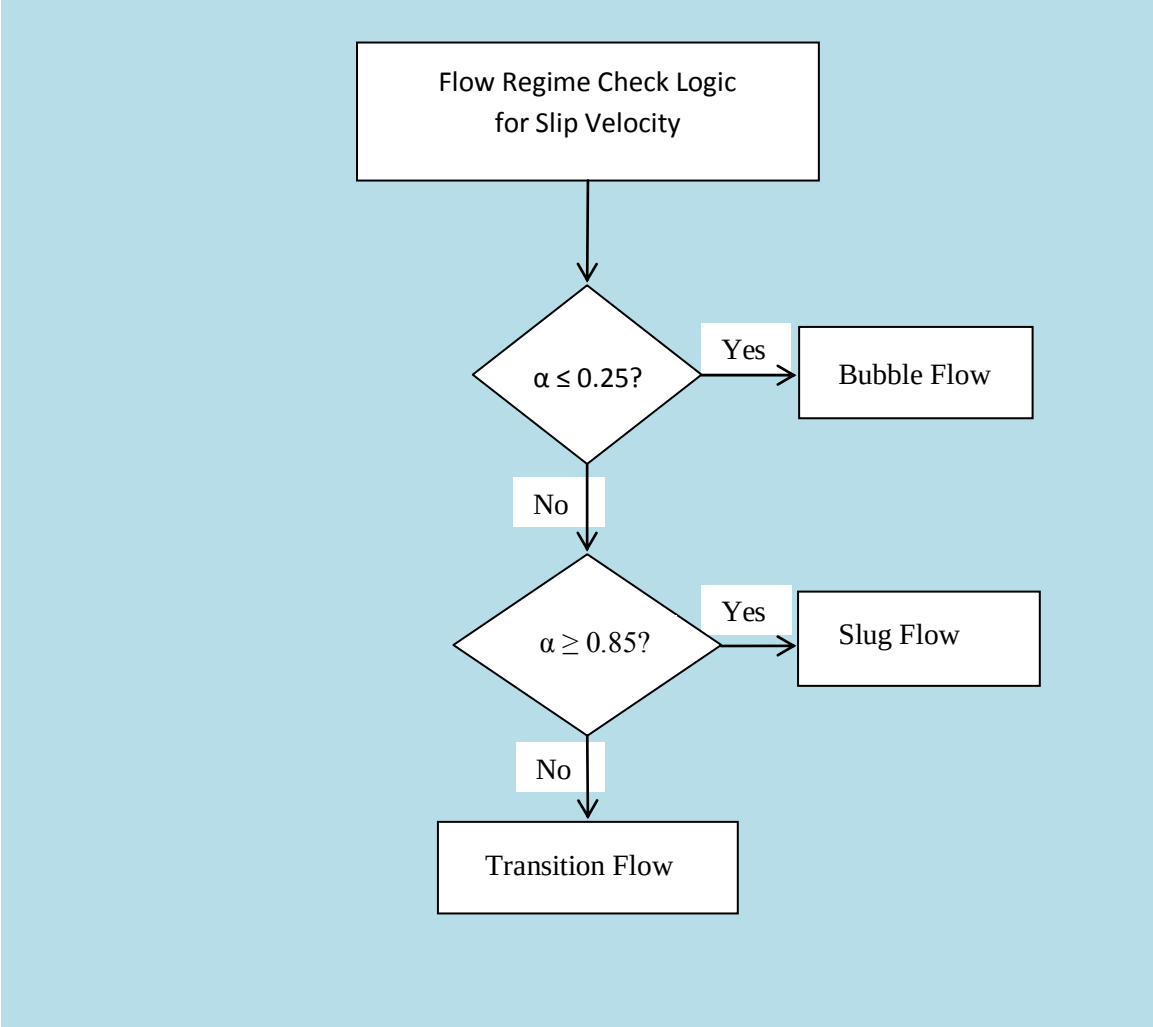

Figure 3.5 Logic for flow regime check to determine slip velocity equation to be applied.

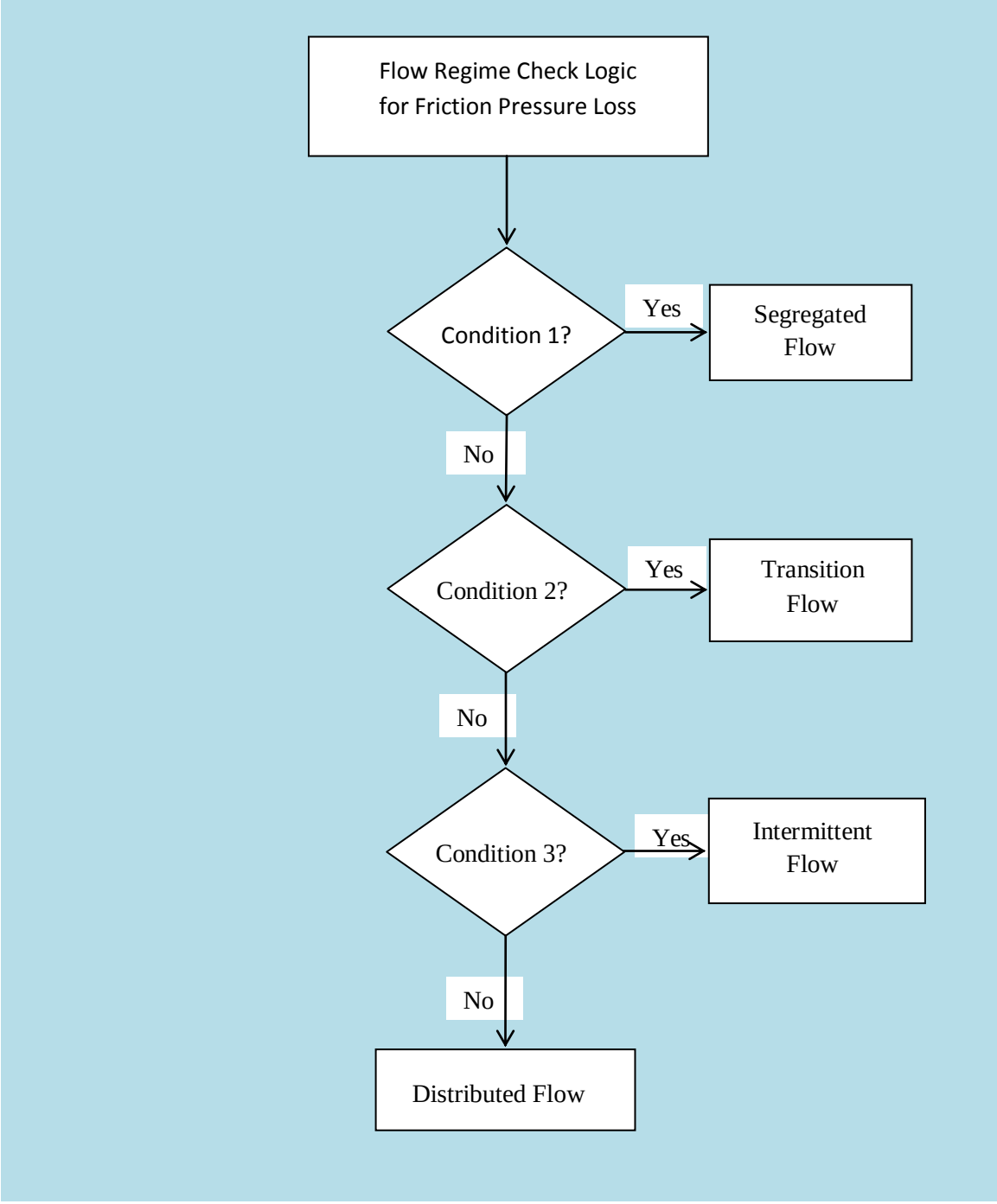

Figure 3.6 Logic for flow regime check to determine the Beggs and Brill constants to be applied.

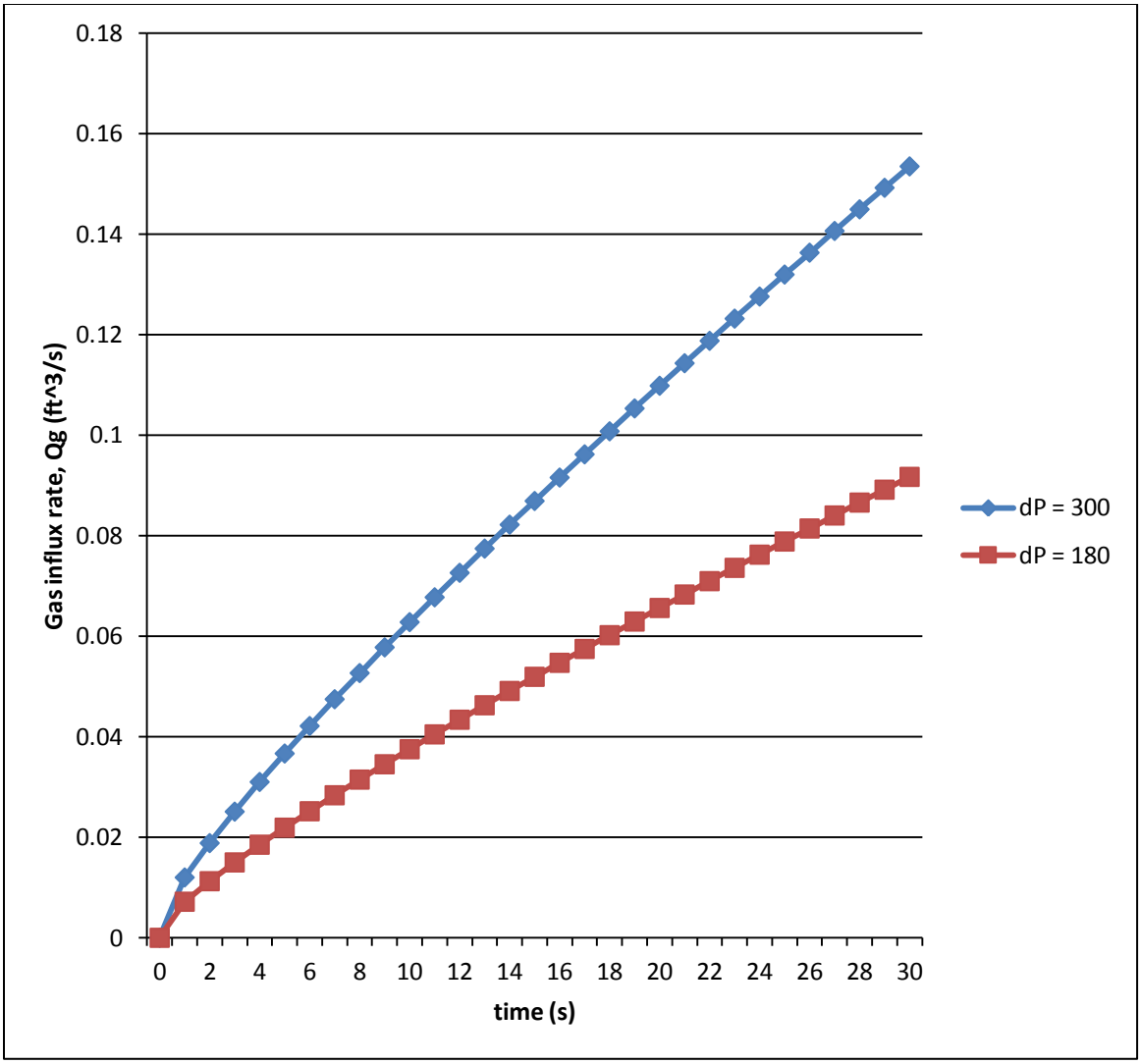

Figure 3.10 Variation of gas influx rate with time at two distinct pressure differentials.

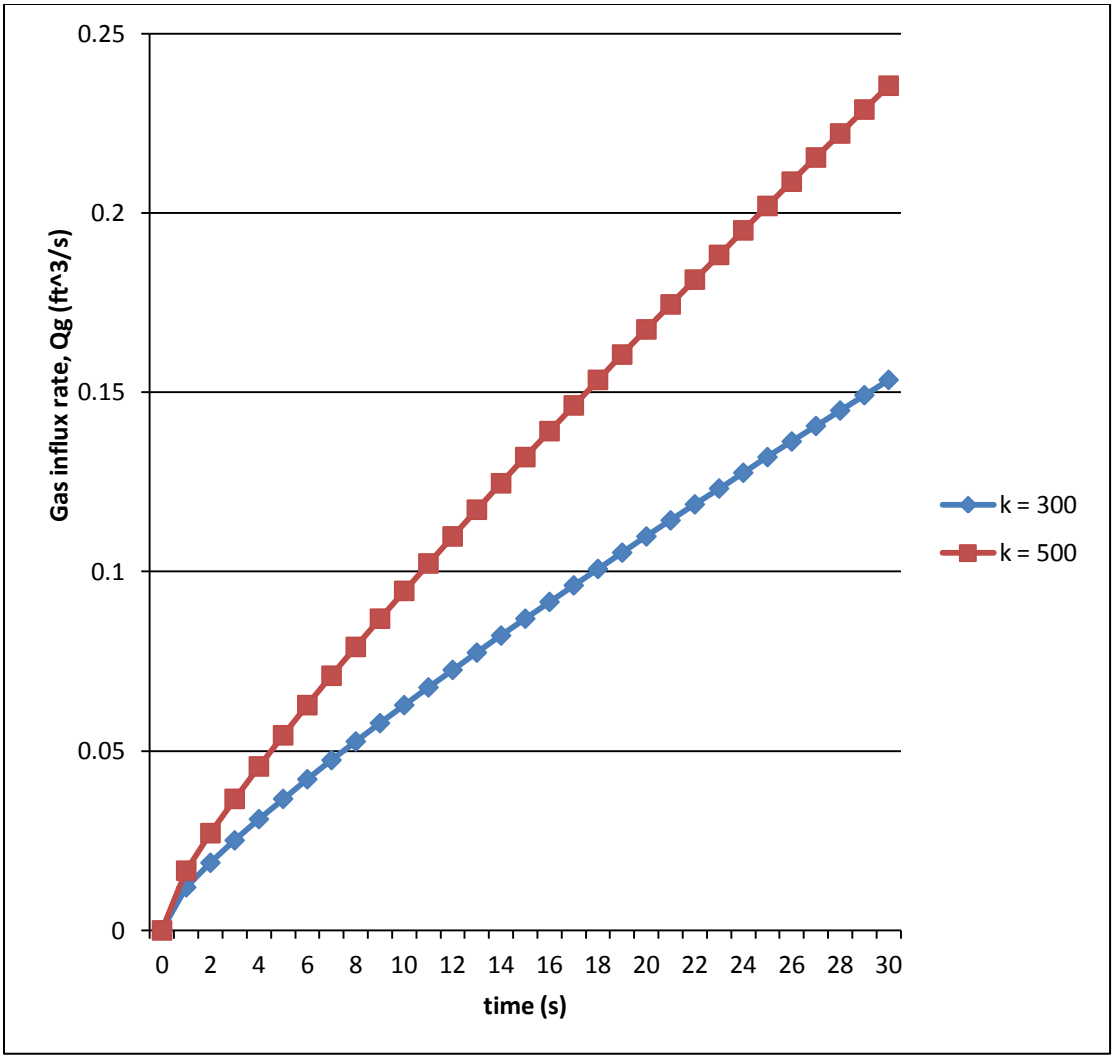

Figure 3.11 Variation of gas influx rate with time at two distinct reservoir permeabilities.

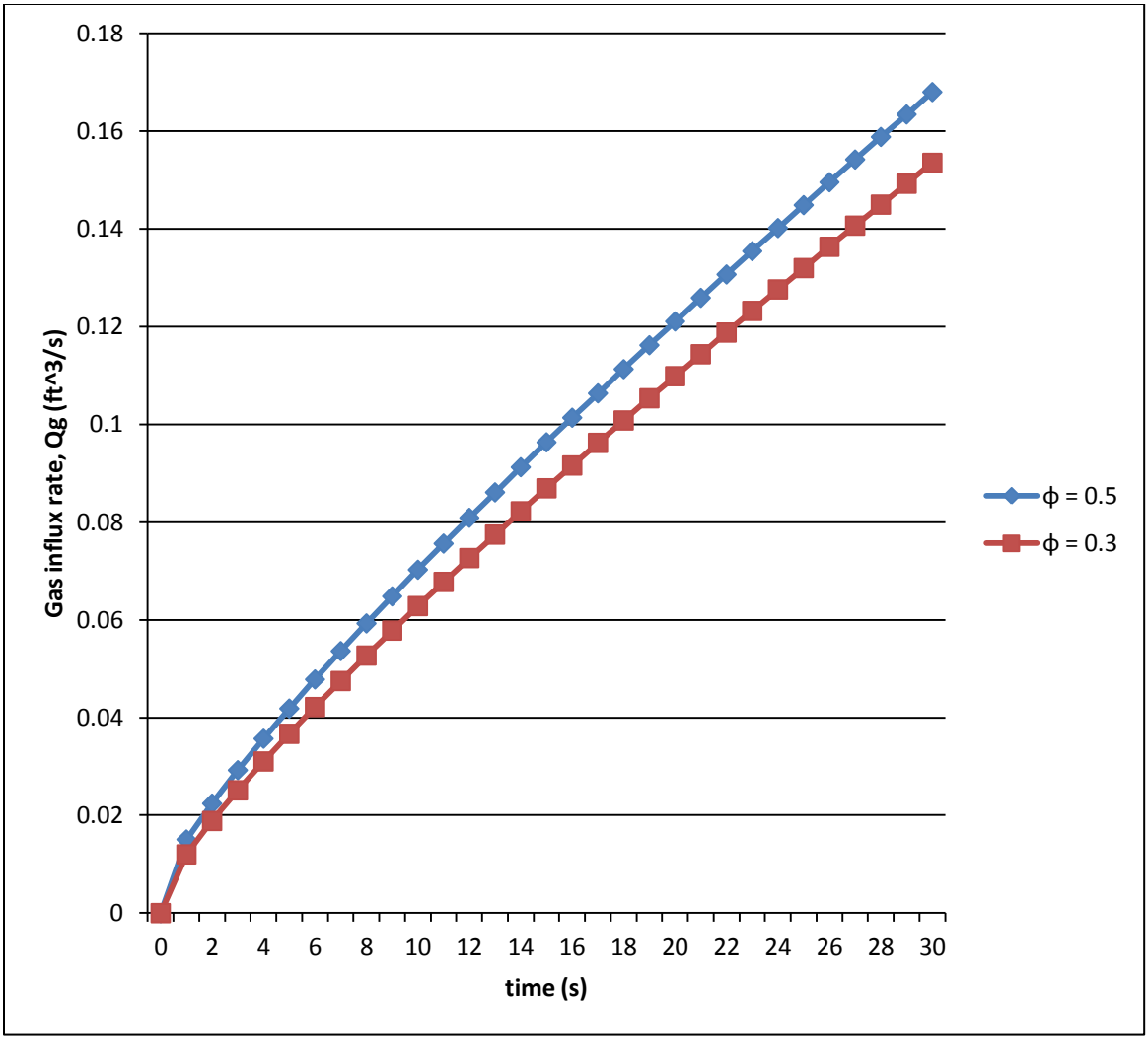

Figure 3.12 Variation of gas influx rate with time at two distinct reservoir porosities.

Chapter 4: Simulation Procedure

The simulation can be done in Matlab, Fortran, C++ or any other simulation software, depending on the capabilities of the user. Many issues may arise with the model during simulation, hence it is best to proceed from lower levels of difficulty to higher levels of difficulty with respect to the number of parameters and variables involved. Aside from providing a good means of tracking and correcting errors as they occur, this gradual introduction of complexity provides better insight into the physics of two phase flows. Accordingly, the following steps are suggested:

1. Start with single phase flow for either gas or mud. This is the simplest case. It involves one continuity equation and a momentum equation for single phase. If single phase mud flow is chosen, it ends up being a steady state system as system parameters are determined at each point on the chosen grid and they do not change with time, given a constant inflow rate. Single phase gas flow is transient because gas influx into the reservoir is a function of time. However, either of these paths, allow for the establishment of a workable grid from the onset. Also, for single phase mud flow, WBM could be modeled as incompressible and later extended to examine compressibility effects. Most of the parameters to be used later are determined at this point, and higher levels of difficulty will mean gradually adding or changing conditions of flow.
2. Extend simulation to multiphase homogenous flow. This involves two continuity equations for mud and gas, and a single momentum equation for the mixture. Homogenous implies that mud and gas are thoroughly mixed and flow with the same velocity. There is no slippage between the phases. Mud could be assumed first as incompressible, and then as compressible. However, this is a transient model with respect to gas kick simulation. The gas void fraction is a function of time, and that impacts the values of the other variables at every point in the grid and as time progresses. For instance, the pressure at a point is a function of the

density of the mixture at that point. As more gas is introduced with time, the density trends downwards and so should the annular pressure. In fact, this is one of the indicators of gas kick: reduced standpipe pressure. As the annular fluid pressure is reduced, the bottomhole pressure is reduced as well, forcing mud from the wellbore into the annulus to balance standpipe and annulus pressures and thus reducing standpipe pressure. This u-tube effect is illustrated in Figure 4.1. The homogenous model allows the establishment of a workable time step for the simulation. According to the Courant-Friedrichs-Lewy (CFL) condition for stability and convergence, the maximum time step is dictated by

$$dt_{max} = \frac{dx_i}{V_i} \quad (1)$$

Where, V_i is the velocity at a grid point. While this is usually applicable to explicit, finite difference numerical methods, it may come in handy as a debugging criteria if the simulation does not converge. Two phase friction pressure loss model is used at this point.

3. Extend simulation to the drift flux model for two phases with the consideration of slippage between the phases. Previously established gridding and time steps are used. Only velocity equations change when the flow regime equations for bubble, slug and transitions flows are introduced. Mud flow may be compressible and/or incompressible.
4. A fourth equation and variable can be introduced at this point - the energy equation which provides the enthalpy at the grid points as a function of time. Once the enthalpy is determined, the temperature profile can be found.

These simulations may be done with the models as explicit, semi-implicit, nearly implicit and fully implicit. The equations derived in Chapter 3 are for the fully implicit model.

4.1 ALTERNATIVE SIMULATION TOOLBOXES

4.1.1 Matlab PDEPE Toolbox

With Matlab, apart from using minimization functions like "fsolve", the tool box "PDEPE" can also be used for partial differential equations modeling. It is used for initial-boundary value problems. The modeler has to first get the equations into the form acceptable to the toolbox, including the initial and boundary conditions. The evolution of the variables with respect to time and space can be plotted in two or three dimensional plots. This may eventually prove easier to use but it provides less insight into the relationships between, and the evolution of variables at the internal grid points as can be seen with the numerical simulation method when debugging.

4.1.2 OLGA/Drillbench SPT Simulation Software

Drillbench is a transient, multiphase flow simulator [39] that captures the physics and complexities of multiphase flows. Features include:

1. Can model in both steady state and transient modes with realistic inputs.
2. Can model three-phase flows - gas, oil, water.
3. Different rheological models can be used for friction pressure loss determination
4. Slip between phases is calculated
5. Output is displayed in time-dependent, easy to read plots
6. Inputs include formation properties, mud properties, drill pipe and annulus dimensions, bit and nozzle area, well depth, temperature profile, inflow rate and outlet and inlet pressures.

It is also suitable for deepwater, High Temperature High Pressure (HTHP) kick modeling. Academic licenses for Drillbench are marketed by the parent company. Apart from the OLGA/Drillbench simulation suite, other similar industry-wide tools exist.

Chapter 5: Summary, Conclusions, Recommendations and Future Work

5.1 SUMMARY

Gas kicks occur as a result of pressure imbalances between wellbore and formation. This often leads to well shut-in and Non-Productive time. If not detected in time and/or left uncontrolled, dangerous and costly blow outs may result. The detection and control of gas kicks is therefore of paramount importance during the drilling of exploration and development wells.

Kick indicators are closely tracked during drilling, tripping and well completions by the drilling crew members in the mud logging unit. While absolute values of drilling parameters are important, what operators often look out for are sharp or gradual changes in these values. Some of the changes are expected during normal drilling operations like pipe tripping, pump shut down/start up, and return flow diversion. Some other changes are unexpected, but merely indicate drilling anomalies like plugged pipe, faulty mud motor, blunt drill bit, etc. Where the aforementioned cases have been ruled out, the drillers must then conclude that unexpected changes may be an indication of gas kick, at which point well control procedures would kick in, in order to prevent blowouts.

Gas kick models provide an insight into the causes, initiation and evolution of gas kicks, and provides the basis for the design of gas kick detection systems. Even where detection systems employ only well data mined from MWD in real-time, mathematical models give an insight into the physical processes taking place and provide the basis for determining appropriate thresholds for system variables before an alarm is made to go off.

This report provides a guide into the architecture of the drilling process, the issues involved with kick detection and control, the modeling of kicks while drilling, the various physical models to consider, the pertinent relationships between parameters and variables, and the discretization of the transient model equations in time and space. A guide to the simulation is also provided and some simulation toolboxes are discussed.

Accurate modeling of the physical processes involved in gas kicks can apart from aiding kick detection, provide the basis for the quantification of gas influxes at the bottomhole in real-time, using statistical and uncertainty techniques like the Monte Carlo method. This work will take this path as it progresses.

5.2 CONCLUSIONS

Literature review suggests that there is still room for improvement in the field of kick detection. While detection after the first 5 to 10 barrels of influx is normal and expected of most systems, the measurements on the basis of which the alarm thresholds are set are taken from surface measurement meters like the flow meter at the return line, level meter in the mud pit and standpipe and annulus pressure sensors. By virtue of the positions of these meters and sensors, there is a time lag between influx at the bottomhole or wellbore open hole and sensing at the meters. This lag is a function of travel time and the fluid properties. Depending on the severity of the kick, control may be difficult and ultimately fail even when detection is early enough.

It is therefore very important to continue improving on detection methods in order to lower alarm thresholds. Already some modern systems boast detection after the first 3 to 5 barrels of influx. MPD systems operate on a much smaller detection scale of 0.5 to 1 barrel of influx. This is impressive. But cost issues and robustness are often a problem.

The modeling of the physical processes involved in gas kicks provide the flexibility to apply the model to different situations: single phase, two and three phase models, homogenous flow, compressible and incompressible flow, drift flux model involving slip between phases, the addition of a temperature variable, among others. This provides greater insight into the physics of the process. Once the chosen model simulation is accurately completed, using statistical approaches to determine the quantity of influx in real time will eliminate lagging issues related to surface measurements and make kick detection faster and well control easier.

5.3 RECOMMENDATIONS AND FUTURE WORK

Chapter 4 details a guide on how to proceed with simulating the model from low to high complexity. This allows for better tracking of errors and better understanding of the physical processes. It also better details the changes that occur from one model to the other. This guide should be adopted.

While it is up to the modeler to determine which discretization method to use, implicit, finite volume numerical analysis often eliminates stability issues when the time step is large, as is the case with finite difference approximations. Also, small time steps generally mean slower simulations, which may end up slower than real time depending on the complexity of the model.

The model complexity adopted should be such as would model all the physics of the process in order to obtain accurate prediction. Hence a realistic model would include gas slip and the appropriate friction pressure loss model which depends on the nature of the flowing fluids. Overly simplified models may simulate faster, but would expectedly yield less accurate results than more complex models.

Separate momentum equations for the two phases should be explored. This would more accurate model the physical process. But care should be taken because the model becomes ill-posed when density and velocity differences between the phases become pronounced [29] and instability results. The circumstances under which this occurs should be studied and avoided.

Also, wall effects could be included in more complex models.

The simulation should also consider the wellbore as either two or three separate regions. Region 1 could be the two phase region of mud and gas at the point of influx and extending as time goes on to the boundary of a single phase region of mud only [31, 32]. The single phase region could be taken as Region 2. Essentially, in region two, the initial conditions of flow still exist (single phase mud flow) as is before the advent of gas kick. Depending on the point of entry of the kick - at the bottomhole or along an open

wellbore section - a single phase mud region could also exist, if the later is the case. This configuration better models the flow dynamics in the well, before and during the gas kick.

As noted earlier, future work will involve the numerical simulation of the discretized models in Matlab and then in C++, and the use of the Monte Carlo quantification technique to predict the number of moles of gas influx at the point of entry.

Glossary

The following symbols list the nomenclature used to represent quantities as used in the text, except where explicitly stated in the text. Field units are used throughout.

A	flow line cross-sectional area (ft^2)
c	calibration constant
cl	mud compressibility constant (psi^{-1})
c_t	reservoir gas compressibility (psi^{-1})
cTl	thermal coefficient of expansion $(^\circ F^{-1})$
d	drillstring diameter (ft)
d_e	annulus outer diameter (ft)
d_i	annulus inner diameter (ft)
d_H	hydraulic diameter (ft)
f	moody friction factor
f_{ns}	no-slip friction factor
F	frictional pressure loss $(lb/ft^2.s^2)$
g	acceleration due to gravity $ft/s^2)$
h	thickness of formation section (ft)
k	reservoir permeability
K	gas pressure constant $(1/ft)$
K_g	gas slip coefficient
M	molecular mass of gas $(lbm/lbmole)$
M_a	molecular mass of air $(lbm/lbmole)$
P	pressure (lb/in^2)
P_{bh}	bottomhole pressure (lb/in^2)
p_D	dimensionless pressure
P_f	formation pressure (lb/in^2)
P_{sc}	pressure at standard conditions $(\frac{lb^2}{in})$
q_g	rate of gas influx from reservoir (ft^3/s)
q_m	rate of flow of mud (ft^3/s)
R	universal gas constant $(psia.ft^3/(lbmole.^\circ R))$
Re	reynold's number
Re_L	reynold's number for laminar flow
Re_T	reynold's number for turbulent flow
ROP	rate of penetration (ft/s)
r_w	wellbore radius (ft)
s	length coordinate (ft)

S skin factor
t time (s)
T temperature $(^{\circ}R)$
t_D dimensionless time
T_{bh} bottomhole temperature $(^{\circ}R)$
v_g flow velocity of gas (ft/s)
v_{gs} relative gas slip velocity (ft/s)
v_m flow velocity of mud (ft/s)
v_{mix} average mixture velocity (ft/s)
x mass fraction of dissolved gas in mud
Y frictional pressure loss $(lb/ft^2.s^2)$
z gas compressibility factor

Greek letters

α void fraction of gas
δ_g specific gravity of gas
θ flow angle with vertical $(rads)$
μ fluid viscosity (cp)
μ_g gas viscosity (cp)
μ_{mix} mixture viscosity (cp)
ρ_{lsc} mud density at standard conditions $(\frac{lb}{ft^3})$
ρ_g gas density $(\frac{lb}{ft^3})$
ρ_m mud density $(\frac{lb}{ft^3})$
φ formation porosity
ϕ mud pressure constant $(1/ft)$

References

1. Choe, J., Schubert, J. J. and Juvkam-Wold, H. C. "Analyses and Procedures for Kick Detection in Subsea Mudlift Drilling", IADC/SPE 87114 prepared for presentation at the IADC/SPE Drilling Conference held in Dallas, Texas, U.S.A., 2-4 March 2004.

2. Rommetveit, R. and Blyberg, A. "Simulation of Gas Kicks During Oil Well Drilling", Modeling, Identification and Control, 1989, Vol. 10, No. 4, 213-225.

3. Maus, L. D., Tannich, J. D., and Ilfery, W. T. "Instrumentation Requirement for Kick Detection in Deep Water", OTC 3240 paper presented at the 1978 Offshore Technology Conference, Houston, May 8-11, 1978.

4. Hargreaves, D., Jardine, S., and Jeffryes, B. "Early Kick Detection for Deepwater Drilling: New Probabilistic Methods Applied in the Field", SPE 71369 prepared for presentation at the 2001 SPE Annual Technical Conference and Exhibition held in New Orleans, Louisiana, 30 September - 3 October, 2001.

5. Wylie, W. W., and Visram A. S. "Drilling Kick Statistic", IADC/SPE 19914 presented at the 1990 IADC/SPE Drilling Conference held in Houston, Texas, 27 February - 2 March 1990.

6. Skalle, P., Jinjun, H. and Podio, A. L. "Killing Methods and Consequences of 1120 Gulf Coast Blowouts During 1960-1990", SPE 53974 presented at the SPE Latin American and Caribbean Conference, Caracas, Venezuela, April, 1999.

7. Orban, J. J., Zanner, K. J., Orban, A. E. "New Flowmeters for Kick and Loss Detection During Drilling", SPE 16665 prepared for presentation at the 62nd Annual Technical Conference and Exhibition held in Dallas, TX, September 27-30, 1987.

8. Gravdal, J. E. "Real-Time Evaluation of Kick Detection During Managed Pressure Drilling Based on Wired Drill Pipe Telemetry", This paper was prepared for presentation at the International Petroleum Technology Conference held in Doha, Qatar, 7-9 December, 2009. IPTC 13959.

9. Austin, E.H. "Drilling Engineering Handbook", IHRDC, 1983.

10. Speers, J. M., and Gehrig, G. F. "Delta Flow: An Accurate, Reliable System for Detecting Kicks and Loss of Circulation During Drilling", SPEDE, December 1987: 359-363.

11. Schafer, D. M., Loeppke, G. E., Glowka, D. A., Scott, D., and Wright, E. K. "An Evaluation of Flowmeters for the Detection of Kicks and Lost Circulation During Drilling", This paper was prepared for presentation at the 1992 IADC/SPE Drilling Conference held in New Orleans, Louisiana, February 18-21, 1992. IADC/SPE 23935.

12. Anfinsen, B. T., and Rommetveit, R. "Sensitivity of Early Kick Detection Parameters in Full-Scale Gas Kick Experiments With Oil- and Water-Based Drilling Muds", IADC/SPE 23934 prepared for presentation at the 1992 IADC/SPE Drilling Conference held in New Orleans, Louisiana, February 18-21, 1992.

13. Santos, H. and Catak, E. "Kick Detection and Control in Oil-Based Mud: Real Well Test Results Using Microflux Control Equipment", SPE/IADC 105454 prepared for presentation at the 2007 SPE/IADC Drilling Conference held in Amsterdam, The Netherlands, 20-22 February 2007.

14. Kamyab, M., Shadizadeh, S. R., Jazayeri-rad, H. and Dinarvand, N. "Early Kick Detection Using Real Time Data Analysis with Dynamic Neural Network: A Case Study in Iranian Oil Fields", SPE 136995 prepared for presentation at the 34th Annual SPE Conference and Exhibition held in Tinapa - Calabar, Nigeria, 31 July - 7 August, 2010.

15. Moheghegh, S., Arefi, R., Ameri, S., and Rose, D. "Design and Development of Artificial Neural Network for Estimation of Formation Permeability", SPE 28237 presented at the SPE Petroleum Computer Conference, Dallas, TX, 31 July - 3 August, 1994.

16. Li, X., Guan, C., Sui, X., and Gangtao. "A New Approach for Early Gas Kick Detection", SPE 50890 prepared for presentation at the 1998 SPE International Conference and Exhibition held in Beijing, China, 2-6 November, 1998.

17. Stokka, S., Andersen, J. O., Freyer, J., and Welde, J. "Gas Kick Warner - An Early Gas Influx Detection Method", This paper was prepared for presentation at the 1993 SPE/IADC Drilling Conference held in Amsterdam, February 23-25, 1993. IADC/SPE 25713.

18. Schubert, J. J., and Wright, J. C. "Early Kick Detection Through Liquid Level Monitoring in the Wellbore", This paper was prepared for presentation at the 1998 IADC/SPE Drilling Conference held in Dallas, Texas, 3-6 March, 1998. IADC/SPE 39400.

19. Santos, H., Leuchtenberg, C. and Shayegi, S. "Microflux Control: The Next Generation in Drilling Process", SPE 81183 prepared for presentation at the SPE Latin American and

Caribbean Petroleum Engineering Conference held in Port-of-Spain, Trinidad, West Indies, 27-30 April 2003.

20. Iversen, F. P., Cayeux, E., Dvergsnes, E. W., Gravdal, J. E. and Vefring, E. H. "Monitoring and Control of Drilling Utilizing Continuously Updated Process Models", IADC/SPE 99207 prepared for presentation at the IADC/SPE Drilling Conference held in Miami, Florida, U.S.A., 21-23 February 2006.

21. Ekrann, S. and Rommetveit, R. "A Simulator for Gas Kicks in Oil-Based Drilling Muds", SPE 14182 prepared for presentation at the 60th Annual Technical Conference and Exhibition of the Society of Petroleum Engineers held in Las Vegas, NV, September 22-25, 1985.

22. Nickens, H.V. "A Dynamic Model of a Kicking Well", SPE, Amoco Production Co, SPE Drilling Engineering, June, 1987.

23. Gravdal, J.E., Lohne, H.P., Nygaard, G., Vefring, E.H. and Time, R.W. "Automatic Evaluation of Near-Well Formation Flow Interaction during Drilling Operations", IPTC 12395 prepared for presentation at the International Petroleum Technology Conference held in Kuala Lumpur, Malaysia, 3-5 December, 2008.

24. Thomas, D.C., Lea, J.F.Jr. and Turek, E.A. "Gas Solubility in Oil-Based Drilling Fluids: Effects on Kick Detection", SPE of AIME, June 1984.

25. Alvaro, F.N. et al “Dynamic Kill of Underground Blowouts”

26. Kelly, M. "Beggs and Brill Method", Lecture Notes, New Mexico Institute of Mines and Technology, 2008.

27. Ashante, B. “Two-Phase Flow: Accounting for the Presence of Liquids in Gas Pipeline Simulation”

28. Turgay, E. et al., "Basic Applied Reservoir Simulation", SPE Book Series, 2001.

29. Mahdy, S. and Sepehrnoori, K. “Development of Transient Mechanistic Two-Phase Flow Model for Wellbores”, SPE 142224 accepted for presentation at the SPE Reservoir Simulation Symposium, The Woodlands, Texas, USA, 21-23 February, 2011.

30. Patankar, S. V. "Numerical Heat transfer and fluid flow", Hemisphere Publishing Corporation, 1980.
31. Avelar, C.S., Ribeiro, P.R., and Sephanoori, K. "Deepwater Gas Kick Simulation", Journal of Petroleum Science and Engineering 67 (2009), 13-22.

32. Starett, M.P., Hill, A.D., and Sepehrnoori, K. "A Shallow Gas Kick Simulator Including Diverter Performance", SPE Drilling Engineering, March 1990

33. Dake, L.P. "Fundamentals of Reservoir Engineering", Elsevier BV, 1978.

34. Brennen, C.E. "Fundamentals of Multiphase Flow", Cambridge University Press, 2005.

35. Guner, H. "Simulation Study of Emerging Well Control Methods for Influxes Caused by Bottomhole Pressure Fluctuations During Managed Pressure Drilling", Thesis, Louisiana State University, Department of Petroleum Engineering, 2009.